Length fluctuations of long cell protrusions: statistics of passage times, random and extremal excursions

Swayamshree Patra¹ and Debashish Chowdhury^{*1}

Department of Physics, Indian Institute of Technology Kanpur, 208016, India

The functional consequences of convenient size of subcellular structures have been analysed in the past and currently the questions regarding the underlying physical mechanisms for their genesis, the sensing of their size by the cell and maintenance of their convenient size in the steady state are receiving much attention. Long cell protrusions, which are effectively one-dimensional, are highly dynamic subcellular structures and their length keep fluctuating about the mean length even in the the steady state. For optimal functioning, particularly as sensors, the length of a specific protrusion must not cross a narrow band bounded by two thresholds. However, fluctuations may drive the length beyond these thresholds. We study generic stochastic models of length control of long cell protrusions: the special cases of this model correspond to specific examples of different types of cell appendages. Exploiting the techniques of level crossings developed for random excursions of stochastic process, we have derived analytical expressions of passage times for hitting various thresholds, sojourn times of random excursions beyond the threshold and the extreme lengths attained during the lifetime of these protrusions. As a concrete example, we apply our general formulae to flagella (also called cilia) of eukaryotic cells thereby getting estimates of the typical length scales and time scales associated with the various aspects of random fluctuations. Since most of the earlier works investigated only the mean length of cell protrusions, our study of the fluctuations opens a new horizon in the field of subcellular size control.

I. INTRODUCTION

Cell is the structural and functional unit of life [1]. For biological function, size matters at all levels of biological organization [2–4]. Even at the subcellular level, each of the structures in an eukaryotic cell has an optimal size [5– 7]. Dynamic long cell protrusions, like eukaryotic flagella and cilia, are effectively linear subcellular structures. The typical length of a particular type of protrusion shows negligible variation across all members of a specific cell type in a given species under same physiological condition. This observation suggests that the individual cells control the length of these structures. What makes these systems attractive in the study of cellular mechanisms for size control is that the the investigator has to deal with an essentially one-dimensional problem [8–25]. Previous studies have focussed on various mechanisms that control mean length of such protrusions. But, to our knowledge, their temporal fluctuations have received very little attention [8, 18].

The temporal fluctuation of the lengths of long cell protrusions may have important implications in their biological functions [26–31]. For example, if the fluctuating length of a sensory cilium falls below a certain threshold it may not be able to pick up molecular signals floating beyond that threshold. When such a situation arises, the shortened cilium becomes silent; the consequent 'fading' of chemical signals received by the cell would be reminiscent of the phenomenon of fading of electromagnetic signals that has been studied extensively [32, 33] since the pioneering work of Rice [34, 35]. The silent cilium

*E-mail: debch@iitk.ac.in

regains its sensory capability only after its length grows above that threshold because of fluctuations. Similarly, growing beyond an upper threshold may lead to excessive exposure to the surrounding environment. This will add to the metabolic cost and disturb the energy budget of the cell [36].

The cell protrusions that motivate this work grow and shrink by assembling or disassembling materials at their distal tips [18]. But, these do not have the machineries of protein synthesis inside the protrusion. Consequently, all the building materials required for elongation of the protrusion need to be imported from the cell body and transported to the distal tip (anterograde transport). Similarly the building materials released from the shrinking distal tip also have to transported back to the cell body (retrograde transport). Transport in both these directions are driven by molecular motors that are powered by a chemical fuel called ATP. Because of the intrinsic stochasticities of the ongoing turnover of the building blocks and incorporation of new materials [8, 37–40], the steady state length keeps fluctuating about the mean (average length) even after the protrusion attains its steady state [41–44]. However, the theory developed in this current paper is not limited to such potrusions. It is applicable to all such protrusion and filaments which grow or shrink by adding or removing monomers from their edges (see Fig.1(a)). For a list of such one dimensional structures, readers are referred to the review article by Mohapatra et al [8].

Steady state length is achieved by striking a balance between the assembly and disassembly of the protrusion [8, 18, 38]. If both these rates are constants and independent of the instantaneous length of the protrusion then, barring an exceptional condition, balance of assembly and disassembly cannot be achieved. To attain

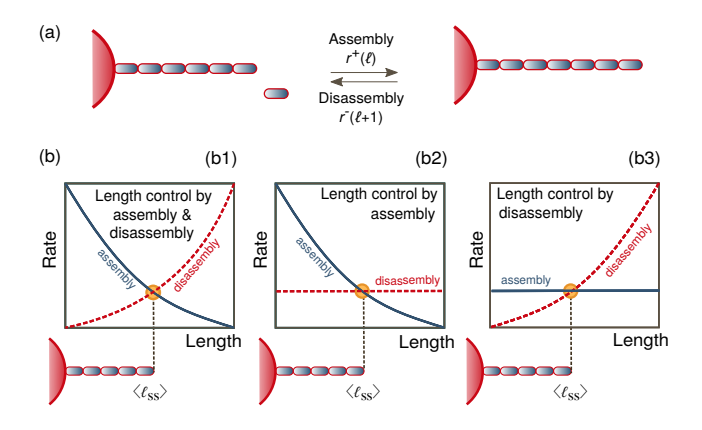


FIG. 1: Length control in generic protrusions and filaments: (a) Generic protrusions and filaments are modelled as lattice chains which can grow or shrink by adding or removing monomers from its end. (b) A controlled length of the structures emerges when the assembly rate is balanced by the disassembly rate. Therefore, for maintaining finite length of the structure (b1) either both the assembly and disassembly rates (b2) or the assembly rate (b3) or the disassembly rate should be dependent on the length of the structure.

a stationary (i.e., time-independent) mean length, either the assembly rate should decrease with increasing length or the disassembly rate should increase with increasing length or both these phenomena must occur. Accordingly, the protrusions can be divided into three classes:

(a) assembly controlled, (b) disassembly controlled and (c) both assembly and disassembly controlled [8] (see Fig. 1(b)).

Length-dependence of the rates of growth and shrinkage of a protrusion can arise from length-dependent regulation of the corresponding anterograde and retrograde transport processes [11]. Alternatively, length-dependence of the shrinking rate of a protrusion can arise from a length-dependent depolymerization of the stiff filaments, that form the cylindrical scaffolding, by specialized enzymes called depolymerases [16, 24, 45]. We will solve the problems for such generic protrusions. However, to get an intuitive feel for the actual numbers, we will apply the analytical formulae derived here exclusively to eukaryotic flagellum which is an example of assembly-controlled protrusion.

The fluctuations of the protrusion length can be viewed as one-dimensional random excursions of its distal tip. If a cell protrusion has certain upper and lower threshold for its lengths, the random excursions of the tip can be formulated as level crossing problems [32, 47–63]. The specific questions we address are: (a) How frequently does the length cross the upper and lower thresholds by fluctuations? (b) What is the duration for which a protusion remains beyond these thresholds? (c) What is the maximum or the minimum length the protrusion can grow or shorten to during its lifetime? Having an estimate for such rates, timescales and lengthscales can help us to get deeper insights into the nature of fluctuations

of the length of cell protrusions.

The manuscript is organised in the following manner. First, we will discuss how to model the assembly and length control of a growing protrusion or filament. It will be followed by the formulation of equations for capturing the stochastic growing shrinking dynamics of these dynamic structures. Thereafter, we show how the fluctuating length of the protrusions and filaments in the steady state can be described by an Ornstein-Uhlenbeck (OU) process. The introduction of length control in eukaryotic flagellum will be followed by the derivation of useful expressions for mean passage times, random excursions and extremal excursions. Finally, using the derived expressions we estimate the level crossing quantities for eukaryotic flagellum. The details of the calculations have been provided in the appendices.

II. EQUATIONS FOR PROTRUSION KINETICS AND FORMAL STEADY STATE SOLUTIONS

The protrusions are modelled here as one-dimensional lattices (i.e., linear chains) of equispaced discrete sites [8, 18]. The growing and shortening of the structures is captured by the addition and removal of monomers from the distal end of the lattice as shown in Fig.1(a).

For these structures to achieve a controlled length, the rate of growing by incorporating new monomers should be balanced by the rate of shortening by discarding the monomers from the structure. This scenario is possible only if both these rates or at least one of them is length dependent. The controlled length emerges where the curves intersect and balance each other (see Fig.1(b)).

The cell assembles protrusions and the filaments from scratch and the average length keep increasing during the growing phase. At some point of time, the average length ceases to change further on the attainment of the steady state. However, the instantaneous length keeps fluctuating about the average length and these length fluctuations are known as steady state length fluctuations.

For the quantitative description of the growing and shrinking dynamics of the generic protrusions, we treat it as a stochastic process L(t) where the stochastic kinetics of the length of the protrusion are assumed to be Markovian. Let $P_L(\ell,t)$ be the probability that the protrusion is of length $L(t) = \ell$ at time t. For simplicity we consider that each monomer is of unit length, so a protrusion of length ℓ consists of ℓ number of monomers.

A. Master Equation for stochastic kinetics: discrete length

The master equation governing the stochastic kinetics [64–66] of the length evolution of the protrusion is given

by

$$\frac{dP_L(\ell,t)}{dt} = r^-(\ell+1)P_L(\ell+1,t) - r^+(\ell)P_L(\ell,t) \text{ for } \ell = 0$$
(1a)

$$\frac{dP_L(\ell,t)}{dt} = r^+(\ell-1)P_L(\ell-1,t) + r^-(\ell+1)P_L(\ell+1,t) - (r^+(\ell) + r^-(\ell))P_L(\ell,t) \text{ for } \ell=2 \text{ to } N-1$$
(1b)

$$\frac{dP_L(\ell,t)}{dt} = r^+(\ell-1)P_L(\ell-1,t) - r^-(\ell)P_L(\ell,t) \text{ for } \ell = N$$
(1c)

where the rate of growing $(r^+(\ell))$ and shortening $(r^-(\ell))$ are length dependent. N denotes the maximum number of monomers which can be incorporated into the protrusion. The motivation for introducing an upper cutoff N for the allowed length of the protrusion is that the pool of structural materials are supplied by the cell body and this supply is finite [5, 6, 68]. Besides, N being a parameter, its magnitude can be varied and adjusted when applied to a specific protrusion.

The steady state solution of the master equation (1) is given by

$$P_s(\ell) = P(0) \prod_{j=1}^{\ell} \frac{r^+(j-1)}{r^-(j)}$$
 (2)

where

$$P(0) = \left(1 + \sum_{\ell=1}^{N} \prod_{j=1}^{\ell} \frac{r^{+}(j-1)}{r^{-}(j)}\right). \tag{3}$$

This gives the distribution of protrusion length in the steady state.

B. Fokker-Planck equation for stochastic kinetics: continuous length

Next we take the continuum limit [64-66] in which the length of the protrusion is represented by a continuous variable y which is defined by

$$y = \ell/N. \tag{4}$$

So the range of allowed values of y is $0 \le y \le 1$. Besides, since both ℓ and N are dimensionless so is y. In this continuum limit, the probability $P_L(\ell,t)$ reduces to p(y,t) which denotes the probability that the protrusion length is y at time t. Carrying out the standard Kramers-Moyal expansion of the master equation (1b) governing the length of the protrusion, we obtain the corresponding Fokker-Planck equation

$$\frac{\partial p(y,t)}{\partial t} = -\frac{\partial}{\partial y} \left[R_{-}(y) p(y,t) \right] + \frac{1}{2N} \frac{\partial^{2}}{\partial y^{2}} \left[R_{+}(y) p(y,t) \right]$$
(5)

where

$$R_{-}(y) = r^{+}(y) - r^{-}(y) \& R_{+}(y) = r^{+}(y) + r^{-}(y)$$
. (6)

Let us rewrite the Fokker-Planck equation (equation (5)) in the following form

$$\frac{\partial p(y,t)}{\partial t} = -\frac{\partial}{\partial y} \left(\underbrace{R_{-}(y(t))p(y,t) - \frac{1}{2N} \frac{\partial R_{+}(y(t))p(y,t)}{\partial y}}_{\mathcal{I}} \right) (7)$$

where the underlined term is the flux \mathcal{J} . In the steady state $\frac{\partial p(x,t)}{\partial t} = 0$ and this indicates that \mathcal{J} is constant. Setting $\mathcal{J} = 0$, we get the steady state solution $p_s(y)$ of the Fokker Planck equation as

$$p_s(y) = \frac{\mathcal{N}}{R_+(y)} \exp\left(2N \int_0^1 \frac{R_-(y')}{R_+(y')} dy'\right)$$
(8)

where \mathcal{N} is the normalization constant.

C. Rate equation for deterministic kinetics: continuous length

From the master equations governing the stochastic time evolution of the length of the protrusions, we get the corresponding rate equation [64–66]

$$\frac{dL(t)}{dt} = r^{+}(L(t)) - r^{-}(L(t)). \tag{9}$$

where $L(t) = \langle \ell(t) \rangle = \sum_{\ell=0}^{N} P_L(\ell, t)$. The steady state solution of the rate equation (9) can be obtained by solving

$$r^{+}(L_{ss}) = r^{-}(L_{ss}) \tag{10}$$

which gives the measure of protrusion length L_{ss} in the steady state.

III. MAPPING PROTRUSION LENGTH FLUCTUATION ONTO OU PROCESS

For the Fokker Planck equation (5), the corresponding stochastic differential equation (SDE) or the Langevin equation [64–66] describing the evolution of the length of the protrusion is given by (see appendix A for the details)

$$dy = R_{-}(y)dt + \frac{1}{\sqrt{N}}\sqrt{R_{+}(y)}dW(t)$$
 (11)

where W(t) is the Gaussian white noise (a Wiener process) with dW(t) distributed according to a Gaussian process with mean and covariance given by

$$\langle dW(t)\rangle = 0$$
 (mean)
 $\langle dW(t)dW(s)\rangle = \delta(t-s)\ dt\ ds$ (covariance) (12)

In the limit $N \to \infty$, from (11) we recover the deterministic equation for y which, after substitutions from (6) and (10), yields the fixed point y^* .

The SDE (11) describing the stochastic evolution of the protrusion length involves Gaussian like fluctuations of order $1/\sqrt{N}$ about the deterministic trajectory. We make a change of variable from y to x by defining $y-y^*=x/\sqrt{N}$ where x is a measure of the deviation of y from its steady-state value y^* . Thus, fluctuations of y around $y=y^*$ is equivalent to that of x around $x^*=0$. Accordingly the functions of $R_{\pm}(y)$ of y get transformed to the functions $\mathcal{R}_{\pm}(x)$ of x. Formally Taylor expanding the RHS of (11) to the lowest order in $1/\sqrt{N}$ (the so-called linear noise approximation [64]) yields

$$dx = \mathcal{R}_{-}(x) dt + \sqrt{\mathcal{R}_{+}(x)} dW(t)$$
 (13)

where

$$\mathcal{R}_{-}(x) = R'_{-}(y^*)x$$
 and $\mathcal{R}_{+}(x) = R_{+}(y^*)$ (14)

The details of deriving equation (13) from equation (11) are given in appendix B.

Note that the transformed Langevin equation (equation (13)) has the formal structure of a standard *Ornstein - Uhlenbeck* (OU) process [69] for which the SDE reads as

$$dx = -\kappa x \ dt + \sqrt{D} \ dW(t); \tag{15}$$

and noise satisfies (12). As is well known, the Fokker-Planck equation corresponding to the SDE (15) is given by

$$\frac{\partial p(x,t)}{\partial t} = \frac{\partial}{\partial x} \left[\kappa x \ p(x,t) \right] + \frac{D}{2} \frac{\partial^2 p(x,t)}{\partial x^2}$$
 (16)

The Fokker-Planck equation corresponding to the transformed Langevin equation (13) for protrusion length is

$$\frac{\partial p(x,t)}{\partial t} = \frac{\partial}{\partial x} \left[\mathcal{R}_{-}(x) \ p(x,t) \right] + \frac{1}{2} \frac{\partial^2 \mathcal{R}_{+}(x) p(x,t)}{\partial x^2}
= \frac{\partial}{\partial x} \left[-R'_{-}(y^*) x \ p(x,t) \right] + \frac{R_{+}(y^*)}{2} \frac{\partial^2 p(x,t)}{\partial x^2} (17)$$

Identifying

$$\kappa = -R'_{-}(y^*) \& D = R_{+}(y^*) \tag{18}$$

we can map the Fokker-Planck equation (17) into OU process (equation (16)).

Rescaling the protrusion length $(y-y^*=x/\sqrt{N})$ and mapping the phenomena into OU process (equation (16) and (17)) allows us to view the movement of the tip about the mean length due to the growing and shortening of the protrusion length as a moving Brownian particle subjected to linear drift (see Fig.2). Note that the allowed range of values of x is $-\sqrt{N} \le x \le \sqrt{N}$. Now to understand the steady state length fluctuations of the protrusion or the dynamics of x, we can use the techniques developed under the framework of OU process to study the dynamics of the Brownian particle which is subjected to linear drift. In table I, we have considered three class of protrusions whose growing and

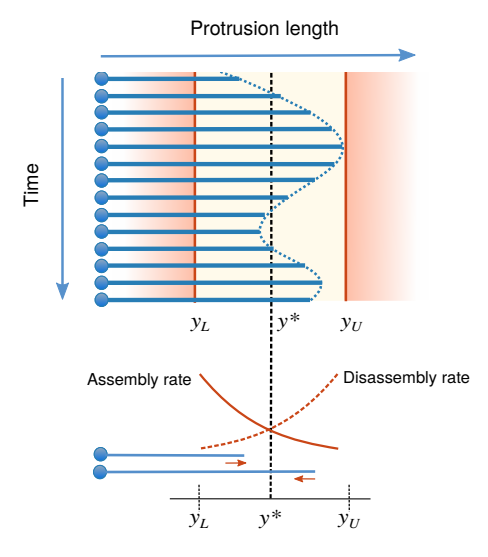


FIG. 2: Fluctuating protrusion length: Protrusion length evolves in time by adding and removing precursors from its tip. The fluctuating protrusion length can be treated as a stochastic process. Due to length dependent assembly and disassembly rate, the protrusion length keeps fluctuating about its mean value in steady state.

shrinking rates are either constant or change linearly with protrusion length. We have summarized the expressions of rates for master equation, rate equations, Fokker-Planck equation and the expression of κ and D when the length fluctuations for these structures are mapped into OU process.

Solutions: The probability distribution $p(x,t|\underline{x_0,t_0})$ by solving the Fokker Planck equation (16) [64–66, 69] reads as

$$p(x,t|\underline{x_0,t_0}) = \sqrt{\frac{\kappa}{\pi D[1 - e^{-2\kappa t}]}} \exp\left(-\frac{\kappa (x - x_0 e^{-\kappa t})^2}{D[1 - e^{-2\kappa t}]}\right)$$
(19

where x_0 is the initial position of the protrusion tip. If the initial mean position is $\langle x_0 \rangle$, the mean position $\langle X(t) \rangle$ evolves as

$$\langle X(t)\rangle = \langle x_0\rangle e^{-\kappa t} \tag{20}$$

and the variance reads as

$$\langle (X(t) - \langle X(t) \rangle)^2 \rangle = \frac{D}{2\kappa} (1 - e^{-2\kappa t})$$
 (21)

The steady state distribution is given by

$$p_{ss}(x) = \sqrt{\frac{\kappa}{\pi D}} \exp\left(-\frac{\kappa x^2}{D}\right)$$
 (22)

and the variance in steady state is given by

$$\sigma^2 = \frac{D}{2\kappa} \ . \tag{23}$$

Quantities	Assembly Controlled	Disassembly Controlled	Assembly-Disassembly Controlled	
Master equation				
$r^{+}(\ell)$	$\lambda_A(N-\ell)$	$\lambda_{ m A}N$	$\lambda_{\mathrm{A}}(N$ - $\ell)$	
r (l)	$\mu_{\mathrm{A}}N$	$\mu_{\rm D}\ell$	$\mu_{ m AD}\ell$	
Rate equation				
$r^+(\langle \ell(t) angle)$	$\lambda_{\mathbf{A}}(1 - \langle \ell(t) \rangle)$	$\lambda_{_{ m D}}$	$\lambda_{AD}(1 - \langle \ell(t) \rangle)$	
$r^-(\langle \ell(t) angle)$	$\mu_{ m A}$	$\mu_{_{\rm D}} \langle \ell(t) \rangle$	$\mu_{\mathrm{AD}}\langle\ell(t)\rangle$	
Fokker -Planck Equation				
$R_{+}(y)$	$\lambda_{A}(1-y)-\mu_{A}$	λ_{D} - $\mu_{\mathrm{D}}y$	$\lambda_{AD}(1-y)-\mu_{AD}y$	
R_(y)	$\lambda_{A}(1-y)+\mu_{A}$	$\lambda_{\mathrm{D}}^{+}\mu_{\mathrm{D}}^{}y$	$\lambda_{AD}(1-y)+\mu_{AD}y$	
Mapping into Ornstein-Uhlenbeck process				
κ	$\lambda_{_{ m A}}$	μ_{D}	$\lambda_{ m AD}^{} + \mu_{ m AD}^{}$	
D	$\mu_{ m A}$	$\lambda_{_{ m D}}$	$[(\lambda_{\mathrm{AD}} \mu_{\mathrm{AD}})/(\lambda_{\mathrm{AD}} + \mu_{\mathrm{AD}})]^{1/2}$	

TABLE I: Summarizing the terms of master equation, rate equation and Fokker-Planck equation for assembly controlled, disassembly controlled and assembly-disassembly controlled protrusions whose rates of assembly and disassembly rates are either constant or linearly changing with the length of the protrusion and listing the expressions of κ and D which are required for mapping the evolution of protrusion length into Ornstein-Uhlenbeck process. Note that λ_s and μ_s are the phenomenological constants which can be extracted from experimental data.

Looking at the expression for $p(x,t|\underline{x_0,t_0})$ and $\langle X(t)\rangle$, the inverse κ^{-1} is actually the timescale with which the protrusion length relaxes to its steady state [69]. The linear drift velocity κx is restoring in nature and always drives the protusion tip towards the mean position x^* , which is the origin $(x^* = 0)$ for the process X(t). More the deviation from the mean position $(x - x^* = x)$, stronger is the drift κx .

The protrusion is growing by adding monomers to its tip and is shortening by removing monomers from its tip (Fig.2). When the assembly rate balances the disassembly rate, a controlled length of the protrusion emerges. If the protrusion grows beyond its controlled (or mean) length, the disassembly rate becomes dominant and forces the protrusion to regain its correct / ideal length by shortening (Fig.2). Similarly, if the protrusion shortens further, the dominant assembly rate helps in reclaiming the correct length by growing. Mapping the growing - shortening dynamics of the protrusion length into the OU process further clarifies the physical picture. It says that the tip keeps doing a random walk by adding and removing subunits but there is always a drift acting on it which drives the protrusion length towards its mean length (or the fixed point x^*).

Whenever we talk about a controlled system undergoing fluctuation, there must be certain upper (x_U) and

lower (x_L) thresholds crossing which may have certain implications (Fig.2). In the coming sections, we will discuss the passage times for hitting the thresholds, the time spent beyond and below these thresholds and the extremum length to which the protrusion can grow or shrink to in a certain interval of time.

IV. A CASE STUDY WITH AN ASSEMBLY CONTROLLED PROTRUSION

For case study, let us consider a protrusion whose length is controlled by assembly. The rate of assembly $(r^+(\ell))$ falls exponentially with the increasing length whereas the rate of disassemly $(r^-(\ell))$ remains constant throughout. Such choice of rates for our model protrusion is motivated by the eukaryotic flagellum [18, 38].

The length dependent growing rate $(r^+(\ell))$ and the length independent shortening rate $(r^-(\ell))$ for our model protrusion are given by

$$r^{+}(\ell) = Ae^{-C\ell} \text{ and } r^{-}(\ell) = B$$
 (24)

where A, B and C are phenomenological constants. If ℓ is converted into proper length by multiplying it with the length $\Delta \ell$ of the subunits of the protrusion, then C must also be divided by $\Delta \ell$ to keep the exponential dimensionless. More about the internal structure, mechanism of acquiring length feedback and how different cytoskeletal and interflagellar components coordinate for assembling flagellum of controlled length will be discussed in section VIII. A more detailed description is provided in our recently published paper [18].

A. Steady state: rate equation approach

Using the general form (10) of the steady-state solution, for our special case (24) under study, we get the steady state mean length to be

$$L_{ss} = \frac{1}{C} log\left(\frac{A}{B}\right) \tag{25}$$

by solving the equation $Ae^{-CL_{ss}} = B$.

B. Steady state: master equation approach

The steady state solution of the master equation (equation (1)) governing the length of the assembly controlled protrusion is obtained by substituting the rates mentioned in equation (24) in the expression mentioned in equation (2) and (3). The following solution of the master equation

$$P_s(\ell) = P(0) \left(\frac{A}{B}\right)^{\ell} e^{-\ell(\ell+1)C/2}$$
(26)

where

$$P(0) = \left(1 + \sum_{\ell=1}^{N} \left(\frac{A}{B}\right)^{\ell} e^{-\ell(\ell+1)C/2}\right)^{-1}$$
 (27)

gives the distribution of the length of the protrusion in the steady state. In terms of A, B and C, the steady state solution of the rate equation (9) governing the length

$$\langle \ell_{ss} \rangle = \frac{1}{C} log \left(\frac{A}{B} \right).$$
 (28)

gives the measure of average length of the assembly controlled protrusion in the steady state. Note that the mean length (28) of the protrusion is identical to the expression (25) of the steady-state length obtained from the rate equation thereby confirming mutual consistency of the two approaches.

C. Steady state and Fluctuations around steady-state: Fokker-Planck approach

For the Fokker-Planck equation (5) governing the evolution of the length of the assembly controlled protrusion, $R_{+}(y)$ and $R_{-}(y)$ are given by

$$R_{+}(y) = Ae^{-Cy} + B \text{ and } R_{-}(y) = Ae^{-Cy} - B.$$
 (29)

Substituting the expressions (29) for $R_{\pm}(y)$ into the general form (8) for the steady state solution, we get

$$p_s(y) = \mathcal{N} \frac{e^{-N\Psi(y)}}{Ae^{-Cy} + B} \tag{30}$$

where the pseudopotential $\Psi(y)$ is given by

$$\Psi(y) = 2 \int_0^1 \frac{R_-(y')}{R_+(y')} dy' = 2 \left(log \left[\frac{Ae^{-Cy} + B}{e^{-Cy}(A+B)} \right] - y \right)$$
(31)

The most probable value of y that, by definition, corresponds to an extremum of the pseudopotential, lies at y^* . Exploiting the definition $y = \ell/N$, we get the most probable length $\ell_{mp} = Ny^*$ of the protrusion in the steady state to be

$$\ell_{mp} = \frac{1}{C} \ell og \left(\frac{A}{B}\right), \tag{32}$$

which is identical to the expressions (25) and (28) of the mean length of the protrusion in the steady-state. Alternatively, from equation (11) in the limit $N \to \infty$ we get the steady-state length to be given by $R_-(y_{ss}) = 0 = Ae^{-Cy_{ss}} - B$, which yields the same expression for the steady-state length as obtained from all the other approaches discussed above. The steady state solution of the master equation, the rate equation and the Fokker Planck equation for the assembly controlled protrusion has been plotted in Fig.3.

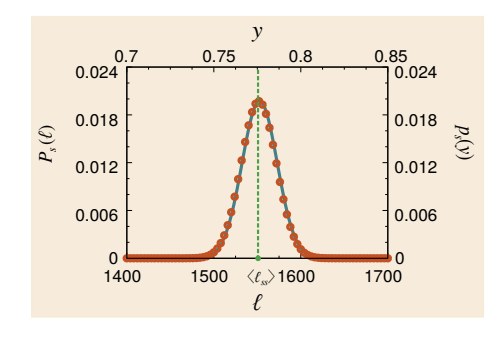


FIG. 3: Steady state solution for model protrusion: The steady state solution of the master equation $(P_s(\ell))$ as a function of ℓ is represented by dots and that of Fokker Planck equation $(p_s(y))$ as a function of y) is represented by the solid blue line. The steady-state length obtained from the rate equation (L_{ss}) , which is identical to the mean length $(\langle \ell_{ss} \rangle)$ obtained from the master equation and the most probable length (ℓ_{mp}) obtained from the Fokker-Planck equation, is marked by the dotted vertical line. Values of $A=1.7\times 10^{-3}$, $B=4.05\times 10^{-5}$ and $C=2.44\times 10^{-3}$ are used for making the plots.

D. Mapping onto OU Process and Fluctuations around steady-state

Substituting the expressions (29) for $R_{\pm}(y)$ in the specific case of assembly-controlled protrusions into the general definitions (18) of κ and D we get

$$\kappa = -R'_{-}(y^*) = BC \text{ and } D = R_{+}(y^*) = 2B.$$
(33)

The Fokker-Planck equation for the transformed Langevin equation (equation (13)) describing the dynamics of the flagellar tip fluctuating about its mean position is given by

$$\frac{\partial p(x,t)}{\partial t} = \frac{\partial}{\partial x} \left[\underbrace{BC}_{\kappa} x p(x,t) \right] + \underbrace{B}_{D/2} \frac{\partial^2 p(x,t)}{\partial x^2} (34)$$

Rescaling the length $(y-y^*=x/\sqrt{N})$ of the assembly controlled protrusion and mapping it into OU process allows us to analyze the system using the techniques developed for OU process.

The length fluctuations, for the initial condition x_0 , are characterized by the probability distribution

$$= \sqrt{\frac{C}{2\pi[1 - e^{-2BCt}]}} \exp\left(-\frac{C(x - x_0 e^{-BCt})^2}{2[1 - e^{-2BCt}]}\right) (35)$$

which, in the limit $t \to \infty$, reduces to the steady-state distribution

$$p_{ss}(x) = \sqrt{\frac{C}{2\pi}} \exp\left(-\frac{Cx^2}{2}\right). \tag{36}$$

V. STATISTICS OF PASSAGE TIMES

One of the central problems of level crossing is estimating the time the system takes to reach a particular boundary for the first time. In the context of a fluctuating protrusion, our interest lies in estimating the time the tip of the protrusion takes to cross a critical value of its length (or, equivalently, the hypothetical Brownian particle takes to cross a threshold boundary) for the first time [46, 55, 57, 60, 62].

Suppose, as shown in figure 4(a), initially the position of Brownian particle (tip) (x_0) lies between two thresholds x_U and x_L ($x_L \leq x \leq x_U$). One of our aims is to calculate the time to escape (or exit) the safe zone, which is bounded by the upper (x_{IJ}) and the lower (x_{IJ}) thresholds, by crossing either of the two thresholds. The time the Brownian particle takes to hit either of the two threshold for the first time defines its first exit time corresponding to the given initial condition. In case there is a single threshold x_{th} ($x_{th} > x^*$) of interest, there are two ways of hitting it (see figure 4(b1-b2)). If the initial position x_0 lies below the threshold x_{th} as shown in figure 4(b1), then it must move upward to hit the threshold length x_{th} and the first time it hits the threshold from below is known as the first upcrossing time. On the otherhand, if x_0 lies above x_{th} (figure 4(b2)), it must move downward to hit the threshold x_{th} ; the first time it hits the threshold x_{th} from above is the first downcrossing time. As we have mapped the movement of the tip onto that of a hypothetical particle that executes an OU process, now we will calculate the mean exit, upcrossing and downcrossing times for the system using the techniques for OU process which are nicely reviewed by Masoliver [46].

Ås is well known, calculation of mean first passage times are normally more convinient if one uses backward Fokker-Planck equation, rather than the forward Fokker-Planck equation given by equation (16) [69]. For the generic model under our consideration, the backward Fokker-Planck equation is given by

$$-\frac{\partial p(x,t|x_0,t_0)}{\partial t_0} = -\kappa x_0 \frac{\partial p(x,t|x_0,t_0)}{\partial x_0} + \frac{D}{2} \frac{\partial^2 p(x,t|x_0,t_0)}{\partial x_0^2}$$
(37)

As both the drift κx_0 and the diffusion D are not dependent on time t and t_0 explicitly, $p(x,t|x_0,t_0)$ depends on time only through the difference $t-t_0$. Therefore, the evolving protrusion length is considered to be temporally homogenous system for which the backward Fokker-Planck equation is given by

$$\frac{\partial p(x,t|x_0,t_0)}{\partial t} = -\kappa x_0 \frac{\partial p(x,t|x_0,t_0)}{\partial x_0} + \frac{D}{2} \frac{\partial^2 p(x,t|x_0,t_0)}{\partial x_0^2} (38)$$

as by chain rule $\partial_{t_0} = -\partial_t$.

The probability that the particle located at x_0 at time t_0 escapes the safe zone, bounded by the upper (x_U) and

the lower (x_L) thresholds, for the first time at time t is given by

$$\mathcal{E}(t; x_U, x_L | \underline{x_0, t_0}) = 1 - \underbrace{\int_{x_U}^{x_L} p(x, t | x_0, t_0) dx}_{\text{probability that the particle is lying between } x_U \text{ and } x_L}_{\text{probability that the particle}}$$
(39)

The probability of hitting a threshold x_{th} is closely related to the escape probability defined in equation (39). Let $\mathcal{H}(t;x_{th}|\underline{x_0,t_0})$ denote the probability of hitting the threshold x_{th} at time t, given that the particle was at x_0 at time t_0 . In case $x_{th} > x_0$, the hitting (or upcrossing) probability is given by

$$\mathcal{H}_U(t; x_{th}|x_0, t_0) = \mathcal{E}(t; x_U = x_{th}, x_L = -\infty | x_0, t_0)$$
 (40)

which is like escaping a semi-infinite interval $(-\infty, x_{th})$. On the other hand, if $x_{th} < x_0$, the hitting (or downcrossing) probability is given by

$$\mathcal{H}_D(t; x_{th}|x_0, t_0) = \mathcal{E}(t; x_U = \infty, x_L = x_{th}|x_0, t_0)$$
 (41)

which is like escaping a semi-infinite interval (x_{th}, ∞) . In the following subsections, we will present the expressions for the mean exit time from the region bounded by two thresholds, the mean hitting time for a given threshold x_{th} and discuss their implications.

A. Escaping the safe zone

The mean escape time taken by the protrusion to grow or shrink beyond x_U and x_L respectively and escaping the safe zone is denoted by

$$\mathcal{T}_{\mathcal{E}}(x_U, x_L | \underline{x_0, t_0}) = \int t \ p_{\mathcal{E}}(t, x_U, x_L | \underline{x_0, t_0}) dt \qquad (42)$$

where $p_{\mathcal{E}}(t, x_U, x_L | \underline{x_0, t_0})$ is the pdf corresponding to the escape probability $\overline{\mathcal{E}(t; x_U, x_L | x_0, t_0)}$. In appendix C1, we have shown that $\mathcal{T}_{\mathcal{E}}(x_U, x_L | \overline{x_0, t_0})$ satisfies the following ordinary differential equation

$$-\kappa x_0 \frac{d\mathcal{T}_{\mathcal{E}}(x_U, x_L | \underline{x_0, t_0})}{dx_0} + \frac{D}{2} \frac{d^2 \mathcal{T}_{\mathcal{E}}(x_U, x_L | \underline{x_0, t_0})}{dx_0^2} = -1$$
(43)

which is subjected to the boundary conditions

$$\mathcal{T}_{\mathcal{E}}(x_U, x_L | x_U, t_0) = 0 = \mathcal{T}_{\mathcal{E}}(x_U, x_L | x_L, t_0). \tag{44}$$

On solving it, we get the expression for the mean escape time $\mathcal{T}_{\mathcal{E}}(x_U, x_L|x_0, t_0)$ which reads as

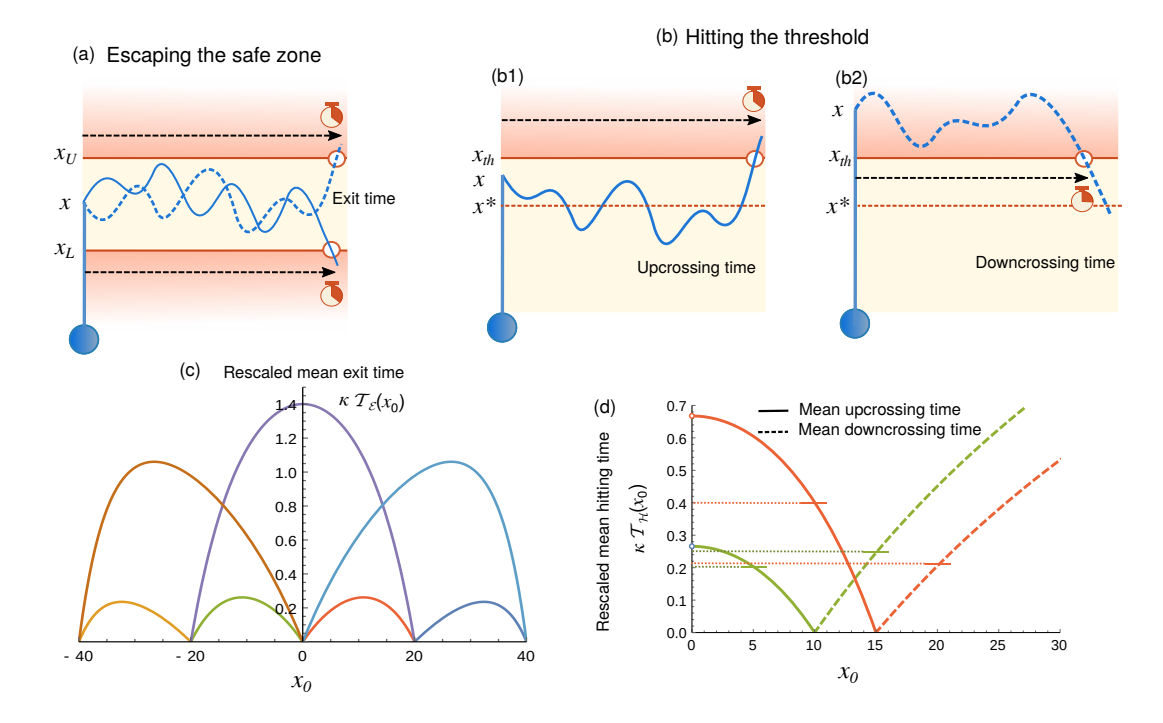


FIG. 4: Statistics of passage time: (a) Space-time diagram for the hypothetical Brownian particle which captures the movement of the tip of the protrusion. It escapes the region bounded by an upper x_U and lower x_L threshold by crossing either of the thresholds and the time taken is the known as the exit time. (b) Space-time diagram for the Brownian particle which lies below (b1) and above (b2) a threshold x_{th} and time taken to hit the threshold is given by upcrossing (b1) and downcrossing (b2) time respectively. (c) Mean exit time for seven different pairs of (x_U, x_L) . (d) Mean upcrossing (solid line) and downcrossing (dashed lines) time for hitting two different threshold $x_{th} = 10$ (green) and $x_{th} = 15$ (red). Value of $\kappa = 9.9 \times 10^{-8}$ and $D = 8.1 \times 10^{-5}$.

$$\mathcal{T}_{\mathcal{E}}(x_{U}, x_{L} | \underline{x_{0}, t_{0}}) = \left[D \left(\operatorname{erfi} \left(\frac{\sqrt{\kappa} x_{L}}{\sqrt{D}} \right) - \operatorname{erfi} \left(\frac{\sqrt{\kappa} x_{U}}{\sqrt{D}} \right) \right) \right]^{-1} \times \left[x_{0}^{2} \left(\operatorname{erfi} \left(\frac{\sqrt{\kappa} x_{U}}{\sqrt{D}} \right) - \operatorname{erfi} \left(\frac{\sqrt{\kappa} x_{L}}{\sqrt{D}} \right) \right) {}_{2}F_{2} \left(1, 1; \frac{3}{2}, 2; \frac{\kappa x_{0}^{2}}{D} \right) + x_{L}^{2} \left(\operatorname{erfi} \left(\frac{\sqrt{\kappa} x_{U}}{\sqrt{D}} \right) - \operatorname{erfi} \left(\frac{\sqrt{\kappa} x_{U}}{\sqrt{D}} \right) \right) {}_{2}F_{2} \left(1, 1; \frac{3}{2}, 2; \frac{\kappa x_{L}^{2}}{D} \right) + x_{L}^{2} \left(\operatorname{erfi} \left(\frac{\sqrt{\kappa} x_{L}}{\sqrt{D}} \right) - \operatorname{erfi} \left(\frac{\sqrt{\kappa} x_{U}}{\sqrt{D}} \right) \right) {}_{2}F_{2} \left(1, 1; \frac{3}{2}, 2; \frac{\kappa x_{L}^{2}}{D} \right) \right] \tag{45}$$

where the function $\operatorname{erfi}(z)$ is the imaginary error function [70] whose series about z=0 is given by

$$\operatorname{erfi}(z) = \frac{1}{\sqrt{\pi}} \left(2z + \frac{2}{3}z^3 + \frac{1}{5}z^5 + \frac{1}{21}z^7 + \dots \right)$$
 (46)

and $_2F_2(a_1, a_2; b_1, b_2; z)$ is the generalized hypergeometric function [70] whose series about z = 0 is given by

$$_{2}F_{2}(a_{1}, a_{2}; b_{1}, b_{2}; z) = \sum_{j=0}^{\infty} \frac{(a_{1})_{j}(a_{2})_{j}}{(b_{1})_{j}(b_{2})_{j}} \frac{z^{j}}{j!}$$
 (47)

In Fig.4(c), we have plotted the mean exit time $\mathcal{T}_{\mathcal{E}}(x_U, x_L | \underline{x_0, t_0})$ as a function of initial position x_0 for seven different pairs of (x_U, x_L) .

B. Hitting the thresholds

If there is a single threshold (x_{th}) of interest, the appropriate quantity is the mean hitting time $\mathcal{T}(x_{th}|x_0,t_0)$ which is the mean time taken to hit the threshold x_{th} for the first time if initially its length is x_0 . The mean hitting time is given by

$$\mathcal{T}_{\mathcal{H}}(x_{th}|\underline{x_0, t_0}) = \int_0^\infty t \ p_{\mathcal{H}}(t; x_{th}|\underline{x_0, t_0}) dt \tag{48}$$

where $p_{\mathcal{H}}(t; x_{th}|\underline{x_0, t_0})$ is the pdf associated with the hitting probability $\overline{\mathcal{H}}(t; x_{th}|\underline{x_0, t_0})$. The steps for deriving the expression of $\mathcal{T}_{\mathcal{H}}(x_{th}|\underline{x_0, t_0})$ are given in the appendix C 2.

For $x_{th} > x_0$ (Fig.4(b1)), the mean hitting or upcrossing time for hitting the threshold is

$$\mathcal{T}_{\mathcal{H}\mathcal{U}}(x_{th}|\underline{x_0, t_0}) = \frac{1}{\kappa} \int_{\kappa x_{th}^2/D}^{\kappa x_{th}^2/D} F(1, 3/2, z) dz = \frac{\sqrt{\pi}}{\kappa} \int_{\sqrt{\kappa}|x_0|/\sqrt{D}}^{\sqrt{\kappa}|x_t|/\sqrt{D}} e^{y^2} \operatorname{erf}(y) dy
= \frac{1}{D} \left[x_{th}^2 {}_2F_2\left(1, 1; \frac{3}{2}, 2; \frac{\kappa x_{th}^2}{D}\right) - x_0^2 {}_2F_2\left(1, 1; \frac{3}{2}, 2; \frac{\kappa x_0^2}{D}\right) \right]$$
(49)

For $x_{th} < x_0$ (Fig.4(b2)), the mean hitting or downcrossing time for hitting the threshold is

$$\mathcal{T}_{\mathcal{H}\mathcal{D}}(x_{th}|\underline{x_0,t_0}) = \frac{1}{2\kappa} \int_{\kappa x_0^2/D}^{\kappa x_0^2/D} U(1,3/2,z) dz = \frac{\sqrt{\pi}}{\kappa} \int_{\sqrt{\kappa}|x_{th}|/\sqrt{D}}^{\sqrt{\kappa}|x_{th}|/\sqrt{D}} e^{y^2} \operatorname{erfc}(y) dy$$

$$= \frac{1}{2\kappa} \left[\pi \operatorname{erfi}\left(\frac{\sqrt{\kappa}x_0}{\sqrt{D}}\right) - \pi \operatorname{erfi}\left(\frac{\sqrt{\kappa}x_{th}}{\sqrt{D}}\right) \right] - \frac{1}{D} \left[x_0^2 {}_2F_2\left(1,1;\frac{3}{2},2;\frac{\kappa x_0^2}{D}\right) - x_{th}^2 {}_2F_2\left(1,1;\frac{3}{2},2;\frac{\kappa x_{th}^2}{D}\right) \right]$$
(50)

In figure 4(d), we have plotted the mean upcrossing (solid line) and downcrossing time (dashed line) for hitting two different thresholds $x_{th} = 10$ (green line) and $x_{th} = 15$ (red line). In equation (49) and equation (50), F(1, 3/2, z) and U(1, 3/2, z) are the generalised Kummer's functions [70].

C. Implications

1. Mean Escape time

The mean escape time plotted as a function of x_0 in Fig.4(c) varies in a non-monotonous manner with the initial position x_0 . The curves in Fig.4(a) exhibit a maximum at x_0^{max} which is given by

$$x_0^{max} = \sqrt{\frac{D}{\kappa}} \times \operatorname{erf}^{-1} \left[\frac{2\kappa}{\pi D} \frac{\left(x_L^2 {}_2F_2\left(1, 1; \frac{3}{2}, 2; \frac{x_L^2 \kappa}{D}\right) - x_U^2 {}_2F_2\left(1, 1; \frac{3}{2}, 2; \frac{x_U^2 \kappa}{D}\right) \right)}{\left(\operatorname{erfi}\left(\frac{\sqrt{\kappa} x_L}{\sqrt{D}}\right) - \operatorname{erfi}\left(\frac{\sqrt{\kappa} x_U}{\sqrt{D}}\right) \right)} \right]$$
(51)

In order to get physical insight into the implications of the exact mathematical expression (48) of $\mathcal{T}_{\mathcal{E}}(x_U, x_L | x_0, t_0)$, let us consider a few special cases all of which place the thresholds symmetrically at equal distances from the origin located at x = 0. The origin x = 0 coincides with the mean position of the Brownian particle (x^*) in the steady-state because $x \propto (y - y^*)$.

Special case I: Suppose, the two thresholds are placed symmetrically at $x_U = a$ and $x_L = -a$, respectively. For this particular positions of the pair of thresholds, the expression (48) for $\mathcal{T}_{\mathcal{E}}(x_U, x_L | x_0, t_0)$ simplifies to

$$\mathcal{T}_{\mathcal{E}}(a, -a|\underline{x_0, 0}) = \frac{1}{D} \left[a^2 \,_2 F_2\left(1, 1; \frac{3}{2}, 2; \frac{a^2 \kappa}{D}\right) - x_0^2 \,_2 F_2\left(1, 1; \frac{3}{2}, 2; \frac{\kappa x_0^2}{D}\right) \right] \tag{52}$$

where x_0 -dependence arises only from x_0^2 appearing in the second term within the square bracket and renders $\mathcal{T}_{\mathcal{E}}(a, -a|\underline{x_0}, 0)$ symmetric with respect to change of sign of x_0 . This symmetry arises from the fact that the distances of the upper and lower thresholds from $x_0 = b$ are identical to those to the lower and upper thresholds, respectively, from $x_0 = -b$. Moreover, not surprisingly, in this symmetric case, the general expression (51) for x_0^{max} coincides with the origin x = 0. In the more general asymmetric case, $\mathcal{T}_{\mathcal{E}}(x_U, x_L|\underline{x_0}, 0)$ is not symmetric. Specializing further to $x_0 = 0$, only the a^2 -dependent first

term within the square bracket in (52) survives while the second term vanishes.

Special case II: A particular lengthscale σ associated with the problem is

$$\sigma = \sqrt{\frac{D}{2\kappa}}. (53)$$

which is obtained by taking the square root of the variance (mentioned in equation (23)) associated with the steady state distribution of X(t) given by equation (22).

Using the series

$$_{2}F_{2}\left(1,1;\frac{3}{2},2;z\right) = 1 + \frac{z}{3} + \frac{4z^{2}}{45} + \mathcal{O}(z^{3})$$
 (54)

we get the approximate expression for $\mathcal{T}_{\mathcal{E}}(a, -a|\underline{x_0, t_0})$ when both x_0 and a are much smaller than σ to be

$$\mathcal{T}_{\mathcal{E}}(a << \sigma, -a << -\sigma | \underline{x_0, t_0}) \approx \frac{1}{D}(a^2 - x_0^2)$$
 (55)

which explains the inverse parabolic form appearing in Fig.4(c). In this special case the mean exit time depends only on D and is independent of κ . The magnitude of the drift in the region $-\sigma < x < \sigma$ is negligible. Therefore, it is diffusion only which drives the escape from this region.

Special case III: Another special case is when $x_U = \sigma$, $x_L = -\sigma$. If in this case $x_0 = 0$, then

$$\mathcal{T}_{\mathcal{E}}(\sigma, -\sigma | \underline{x_0, t_0}) = \frac{0.595}{\kappa}$$
 (56)

i.e., the mean exit time is purely a function of the relaxation time κ^{-1} , irrespective of the magnitude of D.

Special case IV: Suppose the initial position x_0 is very close to one of the boundaries, say x = a while the other boundary is located at x = -a. By the Taylor series expansion of the expression $\mathcal{T}_{\mathcal{E}}(a, -a|\underline{x_0, 0})$ about x = a, we get

$$\lim_{x_0 \to a} \mathcal{T}_{\mathcal{E}}(a, -a | \underline{x_0, t_0}) = \sqrt{\frac{\pi}{D\kappa}} e^{\kappa a^2/D} \operatorname{erf}\left(a\sqrt{\frac{\kappa}{D}}\right) (a - x_0)$$
(57)

i.e., the mean exit time is a linear fuction of the distance $(a-x_0)$ between the initial position and the boundary at x=a. In equation (57) $\operatorname{erf}(z)$ denotes the error function [70] whose series about z=0 is given by

$$erf(z) = \frac{2}{\sqrt{\pi}} \sum_{j=0}^{\infty} \frac{(-1)^j z^{2j+1}}{j!(2j+1)}$$
 (58)

2. Mean Hitting time

The results of mean hitting time (Fig.4(d)) are interesting. Naively, one might expect the mean time for upcrossing the threshold at x_{th} from $x_0 > x_{th}$ to be identical to mean time for downcrossing the same threshold from $x_0 < x_{th}$ if the distance $|x_0 - x_{th}|$ is same in both the cases. But, that is not true, as the detailed analysis of our results (49) and (50) establish.

We plot the results numerically for two different values of the threhold, namely $x_{th} = 10$ and $x_{th} = 15$ in Fig.4(d). For lower threshold $x_{th} = 10$, the mean downcrossing time is longer than the mean upcrossing time (if $|x_0 - x_{th}|$ is same in both the cases) as indicated by the horizontal bars marked on the curve for the mean hitting time for the threshold $x_{th} = 10$ (green curve in figure 4(d)). The opposite is seen for higher threshold $x_{th} = 15$. In this case, the mean upcrossing time is longer than the mean downcrossing time as indicated by the horizontal bars marked on the curve for the mean hitting time for the threshold $x_{th} = 15$ (red curve in figure 4(d)). The reason behind this is the restoring linear drift acting on the tip. In case of lower threshold, the linear drift driving the tip towards mean is weaker. Therefore, it takes longer time for downcrossing the threshold rather than upcrossing it. On the other hand, for higher thresholds, the restoring drift is much stronger. This makes upcrossing a difficult task compared to the downcrossing the threshold. Therefore, the mean upcrossing time is much longer than the mean downcrossing time for a higher threshold.

The expression in equation (49) for mean hitting time of the threshold by upcrossing it is same as the mean escape time given by expression in equation (52) except that a in the later expression (equation (52)) is replaced by x_{th} in the former one (equation (49)). So, in all special cases and special limits, the expression for mean hitting time $\mathcal{T}_{\mathcal{H}\mathcal{U}}(x_{th}|\underline{x_0,t_0})$ resembles $\mathcal{T}_{\mathcal{E}}(x_0;a,-a)$ which are summarised in equation (55-57). On the other hand, the expression for mean hitting time for hitting a threshold by downcrossing it is different so will be the expression for different special cases and in special limits.

In order to gain insight into the physical implications of the mathematical expressions (49) and (50), as before, we consider simple situations. If initially $x_0 = 0$, the mean upcrossing time to any arbitrary threshold x_{th} is

$$\mathcal{T}_{\mathcal{H}\mathcal{U}}(x_{th}|\underline{0,0}) = \frac{x_{th}^2}{D} {}_{2}F_{2}\left(1,1;\frac{3}{2},2;\frac{\kappa x_{th}^2}{D}\right)$$
(59)

whereas if the threshold is $x_{th} = 0$, the mean downcrossing time from any initial location x_0 is

$$\mathcal{T}_{\mathcal{H}\mathcal{D}}(0|\underline{x_0,0}) = \frac{\pi}{2\kappa} \operatorname{erfi}\left(\frac{\sqrt{\kappa}x_0^2}{\sqrt{D}}\right) - \frac{x_0^2}{D} \,_2F_2\left(1,1;\frac{3}{2},2;\frac{\kappa x_0^2}{D}\right)$$
(60)

When both x_0 and x_{th} are much smaller than σ , we use the expansions given in equation (46) and (54) thereby getting the corresponding approximate formulae

$$\mathcal{T}_{HU}(x_{th}|\underline{x_0, t_0}) \approx \frac{1}{D}(x_{th}^2 - x_0^2) \quad (x_0 << \sigma, \text{ and } x_{th} << \sigma)$$
 (61)

for the upcrossing time and

$$\mathcal{T}_{\mathcal{H}\mathcal{D}}(x_{th}|\underline{x_0, t_0}) \approx \sqrt{\frac{\pi}{\kappa D}}(x_0 - x_{th}) - \frac{1}{D}(x_0^2 - x_{th}^2) \quad (x_0 << \sigma, \text{ and } x_{th} << \sigma)$$

$$\tag{62}$$

for the mean downcrossing time. If x_0 is very close to the threshold x_{th} , then the mean upcrossing time is

$$\lim_{x_0 \to x_{th}} \mathcal{T}_{\mathcal{H}\mathcal{U}}(x_{th} | \underline{x_0, t_0}) = \sqrt{\frac{\pi}{D\kappa}} e^{\kappa x_{th}^2 / D} \operatorname{erf}\left(\sqrt{\frac{\kappa}{D}} x_{th}\right) (x_{th} - x_0)$$
(63)

and mean downcrossing time is

$$\lim_{x_0 \to x_{th}} \mathcal{T}_{\mathcal{H}\mathcal{D}}(x_{th} | \underline{x_0, t_0}) = \sqrt{\frac{\pi}{D\kappa}} e^{\kappa x_{th}^2 / D} \left(\left(\operatorname{erf} \left(\frac{\sqrt{\kappa x_{th}}}{\sqrt{D}} \right) - 1 \right) (x_0 - x_{th}) \right)$$
 (64)

and both of these depend linearly on $(|x_0 - x_{th}|)$ which is the distance between the initial position of the tip x_0 and the threshold x_{th} .

Each of the approximate expressions obtained under well defined simple situations expose the inherent asymmetry between the mean times required for hitting threshold from below and from above. This is even more vividly demonstrated by the following consideration. From (49) we extract the mean upcrossing time form $x_0 = 0$ to $x_{th} = \sigma$ and then from $x_0 = \sigma$ to $x_{th} = 2\sigma$. They are

$$\mathcal{T}_{\mathcal{H}\mathcal{U}}(\sigma|\underline{0,t_0}) = \frac{0.595}{\kappa} \text{ and } \mathcal{T}_{\mathcal{H}\mathcal{U}}(2\sigma|\underline{\sigma,t_0}) = \frac{3.90}{\kappa}.$$
 (65)

Similarly, from equation (50) we extract the mean down-crossing time form $x_0 = \sigma$ to $x_{th} = 0$ and then from $x_0 = 2\sigma$ to $x_{th} = \sigma$. They are

$$\mathcal{T}_{\mathcal{H}\mathcal{D}}(0|\underline{\sigma,t_0}) = \frac{0.901}{\kappa} \text{ and } \mathcal{T}_{\mathcal{H}\mathcal{D}}(\sigma|\underline{2\sigma,t_0}) = \frac{0.523}{\kappa}.$$
 (66)

Interestingly, the mean upcrossing time $\mathcal{T}_{\mathcal{H}\mathcal{U}}(\sigma|\underline{0,t_0})$ to upcross form $0 \to \sigma$ is smaller than the mean downcrossing time $\mathcal{T}_{\mathcal{H}\mathcal{D}}(0|\underline{\sigma,t_0})$ to downcross form $\sigma \to 0$. Contrary to this trend, the mean downcrossing time $\mathcal{T}_{\mathcal{H}\mathcal{D}}(\sigma|\underline{2\sigma,t_0})$ to downcross form $2\sigma \to \sigma$ is smaller than the mean upcrossing time $\mathcal{T}_{\mathcal{H}\mathcal{U}}(2\sigma|\sigma,t_0)$ to upcross form $\sigma \to 2\sigma$.

VI. STATISTICS OF RANDOM EXCURSIONS ABOVE A THRESHOLD x_{th}

In the last section, we discussed the distributions of the duration elapsed, from the initial time, before X(t) hits a specific threshold or escapes a safe zone for the first time. In this section, we will again treat the tip of the fluctuating protrusion as a Brownian particle and ask (i) what is the distribution of the number of hits of the given threshold at x_{th} from below (or from above) per unit time, and (ii) what is the distribution of the durations of its sojourn above (or below) the given threshold [32, 34, 35, 61]? For studying the random excursions made by

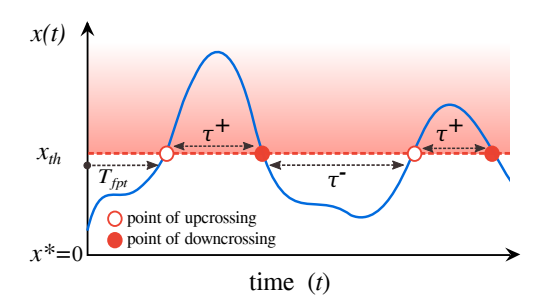


FIG. 5: Random excursion of a Brownian particle: A schematics of the trajectory of a random particle. First time the particle hits the threshold x_{th} is denoted by T_{fpt} . The points of upcrossing the threshold x_{th} are marked by open circles and downcrossing are marked by closed circles. Between and upcrossing and downcrossing, the particle makes a sojourn of duration τ^+ beyond the threshold x_{th} . τ^- denotes the time between two successive excursions beyond the threshold x_{th} .

the fluctuating length of the protrusion in steady state, we will be using the theory of random excursion above a threshold x_{th} which has been developed for OU process by Stratonovich and is well documented in his book [61]. (For a beautiful introduction to random excursion theory, the readers are referred to the book by Brainina [32]).

Terminology for excursion theory: In Fig.5, we have schematically shown a typical trajectory of a Brownian particle and have labelled different quantities of interest which are studied under the random excursion theory. The threshold x_{th} of interest is marked by a horizontal line in Fig.5. τ^+ and τ^- denote the sojourn times above and below, respectively, of the threshold. T_{fpt} is the first passage time for hitting the threshold. We shed light on the statistics of random excursions by computing the (i) mean number of upcrossings of the threshold x_{th} , per unit time and (ii) the distribution of the sojourn times τ^+ for excursions above the threshold x_{th} .

A. Mean rate of upcrossings of threshold x_{th}

Let x_{th} be the threshold of our interest and $x_{th} > x^*$ (see Fig.5). If x denotes the current position of the Brownian particle, the time derivative $\dot{x}(t)$ denotes the rate of change of the position of the Brownian particle with time t. Let $[t, t + \Delta t]$ be such a small interval that the trajectory of the Brownian particle can cross the threshold not more than a single time during this interval. Let P_{1c} denote the probability that the threshold is crossed once and P_{0c} be the probability of no crossing taking place in this small interval. As there are only these two possibilities, the mean number of crossings taking place in this interval is is simply P_{1c} . The probability of crossing the threshold x_{th} in this interval by moving a distance Δx with the velocity lying between \dot{x} and $\dot{x} + \Delta \dot{x}$ is given by

$$dP_c = p(x_{th}, \dot{x}) \Delta x \Delta \dot{x} = p(x_{th}, \dot{x}) \dot{x} \Delta t \Delta \dot{x}$$
 (67)

where $p(x_{th}, \dot{x})$ is the joint distribution of the Brownian particle being at x_{th} whose velocity is $\dot{x}(t)$. We replaced Δx by $\dot{x}\Delta t$ because it is assumed that while moving by a distance Δx , the velocity $\dot{x}(t)$ of the Brownian particle remains constant. Integrating dP_c , we get the total probability P_{1c} of crossing the threshold x_{th} in the interval $[t, \Delta t]$ i.e,

$$P_{1c} = \Delta t \int_0^\infty p(x_{th}, \dot{x}) \dot{x} d\dot{x} . \tag{68}$$

Since, P_{1c} is also the mean number of crossings taking place in this interval, the mean number density of crossing the threshold $n_c(x_{th}, t)$ per unit time is obtained by dividing P_{1c} with Δt . So, the expression for $n_c(x_{th}, t)$ is

$$n_c(x_{th}, t) = \frac{P_{1c}}{\Delta t} = \int_0^\infty p(x_{th}, \dot{x}) \dot{x} d\dot{x}$$
 (69)

As the system is in steady state, $n_c(x_{th}, t)$ will be time independent quantity. Therefore, we use the stationary distribution. Moreover, for an OU process, x and \dot{x} are uncorrelated. Considering these two points, the expression in equation (69) simplifies to

$$n_c(x_{th}) = \int p_{ss}(x_{th}) p_{st}(\dot{x}) \dot{x} d\dot{x}$$
 (70)

which, upon evaluation of the integral, as shown in detail in appendix D 1, leads to

$$n_c(x_{th}) = \frac{\kappa}{2\pi} \exp\left(-\frac{\kappa x_{th}^2}{D}\right).$$
 (71)

In Fig.6(a), we have plotted $n_c(x_{th})$ as a function of x_{th} . In Fig.6(a), we have plotted $n_c(x_{th})$ for three different values of D by keeping κ fixed and in the Fig.6(a) inset, we have plotted $n_c(x_{th})$ for three different values of κ by keeping D fixed. As seen in this figure, the rapid fall of $n_c(x_{th})$ with increasing x_{th} arises from x_{th}^2 in the

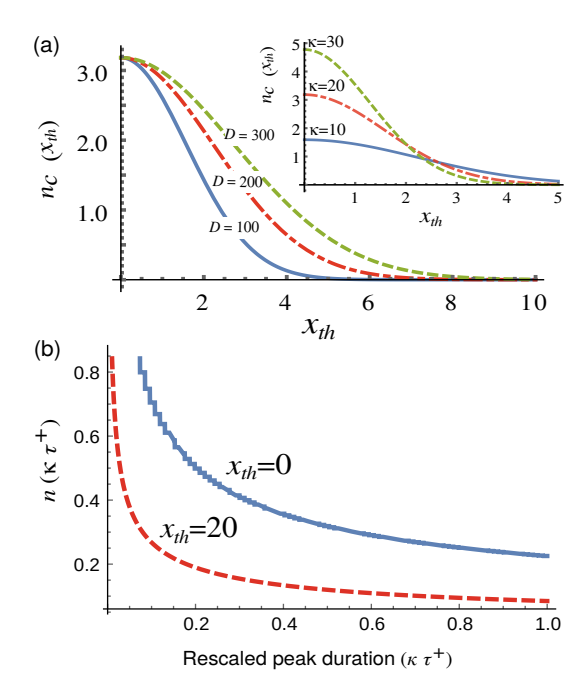


FIG. 6: Quantifying random sojourns: (a) Mean number density $n_c(x_{th})$ (equation (71)) as a function of x_{th} is plotted for fixed $\kappa=20$ and different values of D indicated along the curves. Inset - Mean number density $n_c(x_{th})$ (equation (71)) as a function of x_{th} is plotted for fixed D=100 and for different values of κ indicated along the curves. (b) Mean number of sojourns $n(\kappa \tau^+)$ per unit time is plotted as function of the rescaled sojoun time $\kappa \tau^+$ for two different thresholds - (i) $x_{th}=0$ (solid blue line) and (ii) $x_{th}=20$ (dashed red line). Value of $\kappa=9.9\times10^{-8}$ and $D=8.1\times10^{-5}$ in (b).

factor $exp(-\kappa x_{th}^2/D)$ in Eq.(71). The same exponential factor vividly displays the competing roles of κ and D.

Larger D tends to enhance random excursions away from the steady state. Therefore, for a given κ , higher the value of D, higher is the number density $n_c(x_{th})$ for a given threshold (Fig.6(a)). On the other hand, a stronger κ tends to restore the Brownian particle to its mean position ($x = x^* = 0$). Keeping D fixed, we saw that as we increased the value of κ in Fig.6(a) inset, the curve corresponding to $\kappa = 30$ indicates that the thresholds in the neighborhood of the steady state $x^* = 0$ are more frequently crossed and the crossings become rarer as indicated by the rapidly falling curve for higher x_{th} . For smaller values of κ indicates weaker restoring drift. Therefore, the almost flat curve corresponding to $\kappa = 10$ in Fig.6(a) inset indicates that even the higher thresholds are crossed frequently.

B. Distribution of sojourn times above threshold

We now calculate the mean density of sojourns whose duration exceed τ^+ . This will be followed by the evaluation of the corresponding probability distribution of

sojourn times.

The problem is to count all such trajectories which upcross the threshold x_{th} in the interval $[0, \Delta t]$ and do not downcross it in the next interval $[\Delta t, \tau^+]$. All such trajectories will give rise to sojourns whose duration exceed τ^+ . Let all such trajectories be described by the probability density $p^+(x,t)$. As these trajectories denote fluctuating position of the Brownian particle in time, probability density describing them will satisfy the following Fokker-Planck equation

$$\frac{\partial p^{+}(x,t)}{\partial t} = \frac{\partial}{\partial x} \left[\kappa x \ p^{+}(x,t) \right] + \frac{D}{2} \frac{\partial^{2} p^{+}(x,t)}{\partial x^{2}}. \quad (72)$$

The above equation is subjected to the initial condition

$$p^{+}(x,0) = 0 \text{ for } x > x_{th} \tag{73}$$

and boundary conditions

$$p^{+}(x_{th}, t) = \begin{cases} p_{ss}(x_{th}) \text{ for } 0 \le t \le \Delta t \\ 0 \text{ for } \Delta t < t \end{cases}$$
 (74)

The initial condition (73) indicates that only those trajectories are considered in which the hypothetical Brownian particle is not above the threshold at t=0. The boundary condition (74) in the interval $[0, \Delta t]$ indicates that only those trajectories will contribute which are already at $x = x_{th}$ during the infinitesimal interval $[0, \Delta t]$. As the protrusion length is assumed to be in the stationary state, distribution of such trajectories are given by the stationary distribution $p_{ss}(x_{th})$ given in equation (22). For $t > \Delta t$, the absorbing boundary condition $p^+(x_{th}, t) = 0$ ensures elimination of all those trajectories whose sojourn time above x_{th} would be less than t because of premature downcrossing.

Integration of the probability $p^+(x, \tau^+)$, that satisfies the conditions (73) and (74), over the entire space above x_{th} gives the number of sojourns Δn above threshold which begin in $[0, \Delta t]$ and do not end by $t = \tau^+$, i.e.,

$$\Delta n = \int_{x_{*h}}^{\infty} p^{+}(x, \tau^{+}) dx. \tag{75}$$

Hence, the mean number density of sojourns above the threshold x_{th} , each of duration longer than τ^+ , is given by

$$n(\tau^{+}) = \lim_{\Delta t \to 0} \frac{\Delta n}{\Delta t} \tag{76}$$

The corresponding unnormalised probability density $p_n(\tau^+)$ of the duration of sojourn time above threshold is given by

$$p_n(\tau^+) = -\frac{dn(\tau^+)}{d\tau^+} \tag{77}$$

Solving the equation (72), subjected to the set of conditions given in equation (73) and (74), is a challenging

task. Therefore, we will estimate the sojourn time distributions for two special thresholds $x_{th}=0$ and $x_{th}>>\sigma$ only

Special case I: One of the special cases is to put the threshold at $x_{th} = x^* = 0$. Having X(t) > 0 corresponds to positive excursion whereas X(t) < 0 corresponds to negative excursion. In appendix D 2 we have shown that the number of sojourns of duration longer than τ^+ , above threshold in an unit time interval is given by

$$n(\tau^+) = \frac{\kappa}{\pi} \frac{1}{\sqrt{e^{2\kappa\tau^+} - 1}} \tag{78}$$

Note that $n(\tau^+)$ decreases monotonically with τ^+ . Using (78) in (77) we get the corresponding sojourn time distribution as

$$p_n(\tau^+) = \frac{\kappa}{\pi} \frac{e^{2\kappa\tau^+}}{\left(e^{2\kappa\tau^+} - 1\right)^{3/2}} \ . \tag{79}$$

Special case II: Another class of important thresholds are the ones which are rarely visited $(x_{th}^2 >> D/2\kappa)$, which are rarely visited by the Brownian particle. For such high thresholds $((x_{th}^2 >> D/2\kappa)$, the restoring drift is much stronger. This results in excursions of short duration as the particle will be able to move by a shorter distance beyond x_{th} . Therefore, it is safe to assume that a constant drift of magnitude $\approx |\kappa x_{th}|$ acts on the particle when it is performing excursion beyond the threshold x_{th} i.e, $X(t) > x_{th}$. With this approximation, as shown in appendix D 2, in this special case we get

$$n(\tau^{+}) = \frac{p_{st}(x_{th})}{2} \left[\sqrt{\frac{2D}{\pi \tau^{+}}} e^{-(\kappa x_{th})^{2} \tau^{+}/(2D)} - (\kappa x_{th}) \operatorname{erfc} \left(\kappa x_{th} \sqrt{\frac{\tau^{+}}{2D}} \right) \right]$$
(80)

and

$$p_n(\tau^+) = \frac{p_{ss}(x_{th})}{2} \sqrt{\frac{D}{2\pi}} \frac{1}{(\sqrt{\tau^+})^3} e^{-(\kappa x_{th})^2 \tau^+/(2D)} . (81)$$

Mean number of sojourns per unit time is plotted as function of the rescaled time $\kappa \tau^+$ in Fig.6(b) for two different thresholds - (i) $x_{th} = 0$ (solid blue line) and (ii) $x_{th} = 20$ (dashed red line). For the curve corresponding to $x_{th} = 0$ (solid blue line in Fig.6(b)), we have used the expression of $n(\tau^+)$ mentioned in equation (78) and for the one corresponding to $x_{th} = 20$ (dashed red line in Fig.6(b)), we have used the expression of $n(\tau^+)$ mentioned in equation (80). From Fig.6(b) it is very clear that the number of sojourns of a given duration τ^+ per unit time beyond a lower threshold is more than the number of sojourns beyond a higher threshold. This trend is expected because of the linear nature of the restoring drift which grows stronger with the increasing height of the threshold x_{th} . This prevents excursion of longer duration above higher thresholds. Another inference from Fig.6(b) is that irrespective of x_{th} , the number of sojourns of sojourn time

 τ^+ decrease with increasing sojourn time τ^+ . It is again expected because the restoring drift will ultimately leads to the particle reverting back to its mean position at $x^* = 0$. This property leads to lesser number of sojourns with longer sojourn time.

VII. EXTREMAL EXCURSIONS

After dealing with the theory of random excursions in the last section, now we will discuss one more important aspect of level crossing, namely, the extremal excursions of the protrusion length about its mean length $x^* = 0$ in the steady state. We will look for answers to the questions like what is the maximum or the minimum length the protrusion can grow or shorten to and how wide a range does it scan within a finite duration of time [46, 58, 71]. Again mapping the dynamics of protrusion tip onto that of a Brownian particle executing OU process, we will estimate these important length scales using the theories of extremal excusions developed for OU process in [46].

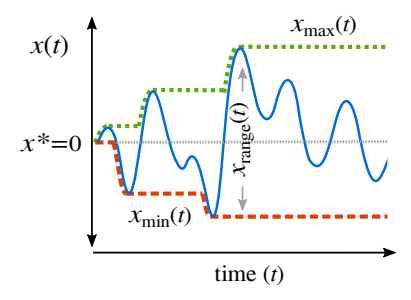


FIG. 7: Extremal excursions: The trajectory of a Brownian particle is denoted by the solid blue line. The evolution of time dependent maximum $x_{max}(t)$ and minimum $x_{min}(t)$ values attained by the Brownian particle are denoted by the dotted green and dashed red line respectively. The range $x_{range}(t)$ spanned is given by the width of the region enclosed by the green dotted line and red dashed line.

A. Average maximum, minimum and range

Let $x_{max}(t)$ and $x_{min}(t)$ be the maximum and the minimum values that the trajectory of the Brownian particle attains at time t. As shown in Fig.7, both $x_{max}(t)$ and $x_{min}(t)$ are time dependent random variables.

The probability of $x_{max}(t)$ being the maximum is denoted by

$$\mathcal{M}_{max}(t; \zeta | \underline{x_0, t_0}) = \text{Probability}[x_{max}(t) < \zeta | \underline{x_0, t_0}]$$
(82)

and the probability of $x_{min}(t)$ being the minimum is denoted by

$$\mathcal{M}_{min}(t; \zeta | \underline{x_0, t_0}) = \text{Probability}[\zeta < x_{min}(t) | \underline{x_0, t_0}].$$
(83)

For simplicity, we will keep our discussion limited to the calculation of statistics of x_{max} . Once we get it for the maximum, getting the results for the minimum x_{min} will be straight forward.

In equation (82), the term Probability $[x_{max}(t) < \zeta | \underline{x_0, t_0}]$ means that the particle which was initially at x_0 $(-\infty < x_0 < \zeta)$ has not escaped the region $[-\infty, \zeta]$. In other words, it has not hit the threshold $x_{th} = \zeta$ till time t. Therefore,

$$\mathcal{M}_{max}(t;\zeta|x_0,t_0) = (1 - \mathcal{H}_U(t;\zeta|x_0,t_0))\Theta(x_0 - \zeta)$$
. (84)

where $\mathcal{H}_U(t;\zeta|x_0,t_0)$ is the upcrossing probability for the threshold ζ which was introduced in equation (40). The heaviside function $\Theta(x_0-\zeta)$ takes care of the fact that if initially the particle is located beyond ζ , then it is impossible to have ζ as the maximum. As the pdf corresponding to $\mathcal{M}_{max}(t;\zeta|x_0,t_0)$ is $p_{max}(t;\zeta|x_0,t_0)$, the mean maximum $\langle x_{max}(t)|x_0\rangle$ is given by

$$\langle x_{max}(t)|x_0\rangle = \int_0^\infty \zeta \ p_{max}(t;\zeta|\underline{x_0,t_0}) \ d\zeta \ . \tag{85}$$

Rather than having arbitrary values of x_0 , we fix $x_0=0(=x^*)$ without loss of generality. This will give us the average maximum excursion $\langle x_{max}(t)|x_0\rangle$ about the mean position $x^*=0$ in steady state. As derived in detail in appendix E, it is shown that the average maximum $\langle x_{max}(t)|0\rangle$ goes as

$$\langle x_{max}(t)|0\rangle \simeq \sqrt{\pi Dt}$$
 (86)

i.e, the $\langle x_{max}(t)|0\rangle \propto \sqrt{Dt}$.

Next, let us calculate $\langle x_{min}(t)|0\rangle$. If initially $x_0 = 0$, then $\langle x_{min}(t)|0\rangle$ is related to the first downcrossing time to $x_{th} = -\zeta$. We also know that

$$\mathcal{H}_D(t; -\zeta | 0, t_0) = \mathcal{H}_U(t; \zeta | 0, t_0).$$
 (87)

Therefore, without going through detailed calculations again, we can simply write

$$\langle x_{min}(t)|0\rangle = -\langle x_{max}(t)|0\rangle = -\sqrt{\pi Dt}$$
. (88)

The range scanned by the Brownian particle, as shown schematically in Fig.7, is a time dependent random variable that depends on both $x_{max}(t)$ and $x_{min}(t)$. The average width of the range is denoted by $\langle x_{range}(t)|0\rangle$. It can be evaluated directly by subtracting the average minimum from the average maximum i.e,

$$\langle x_{range}(t)|0\rangle = \langle x_{max}(t)|0\rangle - \langle x_{min}(t)|0\rangle = 2\sqrt{\pi Dt}$$
 (89)

B. Implications

At first it is surprising that all the three quantities $\langle x_{max}(t)|0\rangle$, $\langle x_{min}(t)|0\rangle$ and $\langle x_{range}(t)|0\rangle$ (see equation (86),(88) and (89)) characterizing the extremal excursions are proportional to \sqrt{Dt} just like the root mean

square displacement in pure diffusion. The most interesting feature of these expressions for the three quantities is that none of these depend on κ at all. Since it is solely because of diffusion that the particle tends to move away from the mean position and explore extremes, all these three time-dependent quantities vary with time as \sqrt{Dt} , the hall mark of diffusion.

VIII. EUKARYOTIC FLAGELLUM: A CASE STUDY

Internal structure: Eukaryotic flagellum is a membrane bound organelle that projects out of the cell body. The primary structural scaffold which forms the flagellum is the axoneme [72]. Axoneme is a microtubule (MT)-based structure consisting of nine MT doublets and 2 single MTs (see Fig.8). The doublets are arranged in a cylindrical fashion with the two singlets at the center. Absence of mRNAs inside the flagellum indicates that the flagellum imports its structural proteins (now onwards, loosely, referred to as "precursor") from the cell body. The flagellar precursors are synthesized and and degraded in the pool which is situated at the flagellar base [72].

Intraflagellar transport: An active transport mechanism known as intraflagellar transport (IFT) is responsible for transferring precursors into and out of the flagellum [74–76]. IFT trains consist of IFT proteins which are arranged in linear arrays just like the bogies of a train (see Fig.8). These are pulled by molecular motors which walk on the MT doublets. The precursors hitchike on these trains to get a ride inside the flagellum. One of the MTs of the doublet (B-MT) is exlusively used for the anterograde trip of the IFT trains to the tip and the other one (A-MT) is used for the retrograde trip from tip to the base [77]. The IFT trains are driven towards the flagellar tip by the kinesin motors. At the tip, the trains get 'remodelled', kinesins are 'disengaged' and the dynein motors get 'activated'. Thereafter, they are pulled back to the base by the dynein motors. Due to the use of separate MTs, anterograde and retrograde trains never collide.

Length control: A flagellum elongates by incorporating the precursors, which are brought by the IFT trains, at its tip. Because of the turnover of tubulins at the flagellar tip, the flagellum shortens by removal of precursors [11, 38, 72, 78]. The overall assembly rate decreases with the increasing flagellar length whereas the disassembly rate remains constant throughout the process [11, 38, 72, 78]. A steady state length emerges by the balance of elongation and retraction. According to the differential loading model, the amount of precursors loaded onto an IFT train decreases with the increasing length of the flagellum and this is responsible for the overall decrease in the assembly rate with the growing length of the flagellum. The cell senses the flagellar length with a "time of flight" mechanism [11, 18, 78].

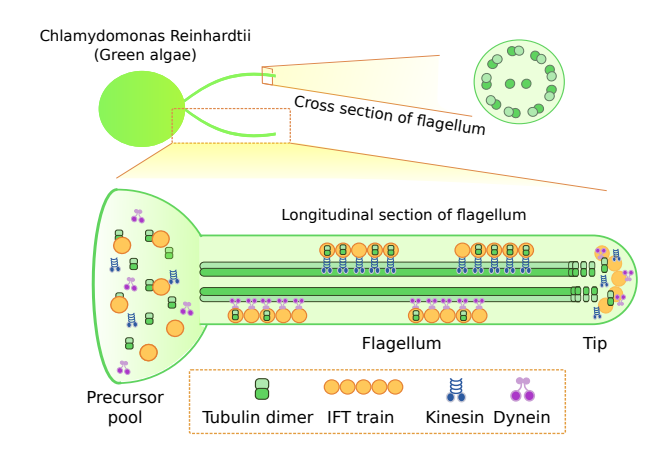


FIG. 8: A glimpse into the internal structure of flagellum and elements of intraflagellar transport.

Suppose, the timer molecule, which is an integral part of the IFT trains, enters the flagellum in a particular chemical (or, conformational) state. It can switch irreversibly to another state at a certain rate. The state of the timer molecule, which finishes the roundtrip inside the flagellum, gives a feedback to the cell as to the current flagellar length. Longer the flagellum, longer the time of flight and higher is the probability of flipping of the state of the timer. If the timer returns to the base with its state unchanged, then it implies that precursors have to be loaded on to next IFT train, but otherwise no cargo is loaded onto the next IFT train that starts its round trip inside the flagellum.

Model: Here we summarize the key points of a stochastic model that we have developed very recently for studying flagellar length control (see [18] for the details). The flagellum is represented as a pair of antiparallel lattices, where each lattice represents a MT of the doublet. IFT particles pulled by the motors are represented by self driven particles which obey exclusion principle and jump to the neighboring sites in a stochastic manner with a certain hopping rate. The flux of the IFT particles inside the flagellum is J, their number density on the lattice is ρ and the effective velocity with which they move is v. Each IFT particle can be either empty or loaded with a single lattice unit which can elongate the model flagellum (pair of lattices) at the tip by a single unit. Whether the IFT train is loaded or not with a lattice unit depends on the state of the timer and the amount of precursor in the pool. If initially the timer is in a given state, the probability of finding the timer in the same state after time t is given by exp(-kt) where k is rate of flipping of the state of the timer. So, if the flagellar length is L(t) at time t, the probability of the timer returning to the base (after the roundtrip inside flagellum) without flipping state is $e^{-kt_{tof}}$ where t_{tof} is the time of flight and is given by $t_{tof} = 2L(t)/v$. So far as the precursor pool is concerned, if the maximum capacity of pool is N_{max} and by some mechanism the cell maintains a steady amount of precursors N_{ss} in the pool

then the probability of loading of precursors onto an IFT train is proportional to N_{ss}/N_{max} . Therefore the flux of full trains reaching the flagellar tip is

$$J_{full} = \frac{N_{ss}}{N_{max}} e^{-2kL(t)/v} J \tag{90}$$

The precursor loaded on the IFT train can elongate the flagellum with probability Ω_e . So the overall rate of assembly is given by

$$J\Omega_e \ e^{-2kL(t)/v}. (91)$$

Due to ongoing turnover, if both the sites at the tip are not occupied by any IFT trains, the dimer (i.e the precursor) dissociates with rate Γ_r . Therefore, the overall disassembly rate is given by

$$(1-\rho)^2 \Gamma_r \tag{92}$$

The stochastic time-evolution of the flagellar length can be modelled by a a master equation (1) with the corresponding rates

$$r^{+}(\ell) = Ae^{-C\ell} \quad \text{and} \quad r^{-}(\ell) = B \tag{93}$$

where

$$A = \frac{N_{ss}}{N_{max}} J\Omega_e, \ B = (1 - \rho)^2 \Gamma_r \& C = 2k/v.$$
 (94)

A. Parameter estimation for eukaryotic flagellum

Now we estimate the model parameters relevant for the steady state length fluctuations of the flagellum of Chlamydomonas reinhardtii. We chose this species because the flagellum of this particular species of green algae is most commonly used in experimental studies of length control [11, 38, 78]. Based on our earlier experience of analysis of experimental data for [18], we fix $A=809.6~\mathrm{min}^{-1},~B=28.21~\mathrm{min}^{-1}$ and C=0.0021 which appear in equation (93). We solve for the evolution of mean flagellar length $\langle \ell(t) \rangle$ using equation (9) and multiply $\langle \ell(t) \rangle$ with 8 nm for converting it into actual length; 8 nm being the length of a single MT dimer. Plugging the values of A, B and C in the expressions in equation (33), we get the corresponding values of

$$\kappa^{-1} = (BC)^{-1} = 16.3 \text{ minutes}$$
(95)

and

$$D = 2B = 56.42 \text{ min}^{-1} \tag{96}$$

which are the two essential parameters of the OU process. Note that the mean length in steady state for the flagellum is

$$\langle \ell_{ss} \rangle = \frac{1}{C} log \left(\frac{A}{B} \right) = 12.3 \ \mu m,$$
 (97)

which is, indeed, the typical length of a flagellum of *Chlamydomonas reinhardtii*, and

$$\sigma = \sqrt{\frac{D}{2\kappa}} = \sqrt{\frac{1}{C}} = 0.17 \ \mu m \tag{98}$$

B. Level-crossing statistics for eukaryotic flagellum

First we estimate the mean hitting times for a flagellum of *Chlamydomonas reinherdtii* using the expressions of hitting times (65,66) derived in section V. The mean hitting time for important thresholds is listed in Fig.9(b) and the timescales are presented in measurable units (in minutes). The mean time taken by the flagellar length to hit the threshold $\langle \ell_{ss} \rangle + \sigma$ is around 10 minutes whereas the mean time to regain the mean length $\langle \ell_{ss} \rangle$ is around 15 minutes. Notice the asymmetry in mean times in hitting equidistant thresholds in opposite directions.

Moreover, it takes around 1 hour, on the average, to grow from $\langle \ell_{ss} \rangle + \sigma$ to $\langle \ell_{ss} \rangle + 2\sigma$ by fluctuations whereas it can shorten to $\langle \ell_{ss} \rangle + \sigma$ from $\langle \ell_{ss} \rangle + 2\sigma$ in around 8 minutes, on the average. From the estimates of hitting time, it is concluded that upcrossing from $\langle \ell_{ss} \rangle + \sigma$ to $\langle \ell_{ss} \rangle + 2\sigma$ is more difficult than downcrossing from $\langle \ell_{ss} \rangle + \sigma$ to $\langle \ell_{ss} \rangle + \sigma$ whereas downcrossing from $\langle \ell_{ss} \rangle + \sigma$ to $\langle \ell_{ss} \rangle$ is more challenging than upcrossing from $\langle \ell_{ss} \rangle$ to $\langle \ell_{ss} \rangle + \sigma$.

Next we estimate the number density of threshold crossings and the sojourn times above a threshold, which are statistical properties of random excursions discused in section VI. The mean number $n_c(x_{th})$ of times a given threshold x_{th} is crossed per minute (see expression (71)) is plotted as a function of $x_{th} - \langle \ell_{ss} \rangle$ in Fig.9(c1). The number of crossings per minute of the particular threshold $x_{th} - \langle \ell_{ss} \rangle = \sigma$ is also marked in Fig.9(c1). Again, the decreasing trend of the curve reconfirms the fact that upcrossing the higher thresholds is more difficult and rare. We have also estimated the number of sojourns $n(\tau^+)$ above a threshold x_{th} per minute whose duration exceed τ^+ (in minutes). We get the estimate for three special thresholds (i) $x_{th} = 0$, (ii) $x_{th} = \langle \ell_{ss} \rangle + \sigma$ and (iii) $x_{th} = \langle \ell_{ss} \rangle + 2\sigma$. Using the expressions (78) and (80), we plot $n(\tau^+)$ as a function of τ^+ for these three thresholds. For all the three threshold, $n(\tau^+)$ decrease with increasing τ^+ indicating that number of sojourns with sojourn time longer than τ^+ decrease with increasing τ^+ .

Finally, we address the questions on the maximum and minimum lengths a flagellum can attain during its lifetime merely by fluctuations beginning from its steady-state. For this purpose we get the relevant estimates by using the expression (86),(88) and (89). Chlamydomonas reinhardtii assembles its flagellum at the beginning of G1 phase of the cell cylce and starts to disassemble at the end of this phase when the cell prepares itself for cell division. G1 phase lasts for 10-12 hours. About its steady state length $\langle \ell_{ss} \rangle \approx 12 \mu m$, the maximum and minimum average length by which the flagellum can grow or shorten during its lifetime of 10 hours is $2.5 \mu m$ i.e, it can grow to $\approx 14.8 \mu m$ and shorten to $\approx 9.8 \mu m$ due to length fluctuation in 10 hours. The range scanned by the flagellar tip during its lifetime is, thus, about $5 \mu m$.

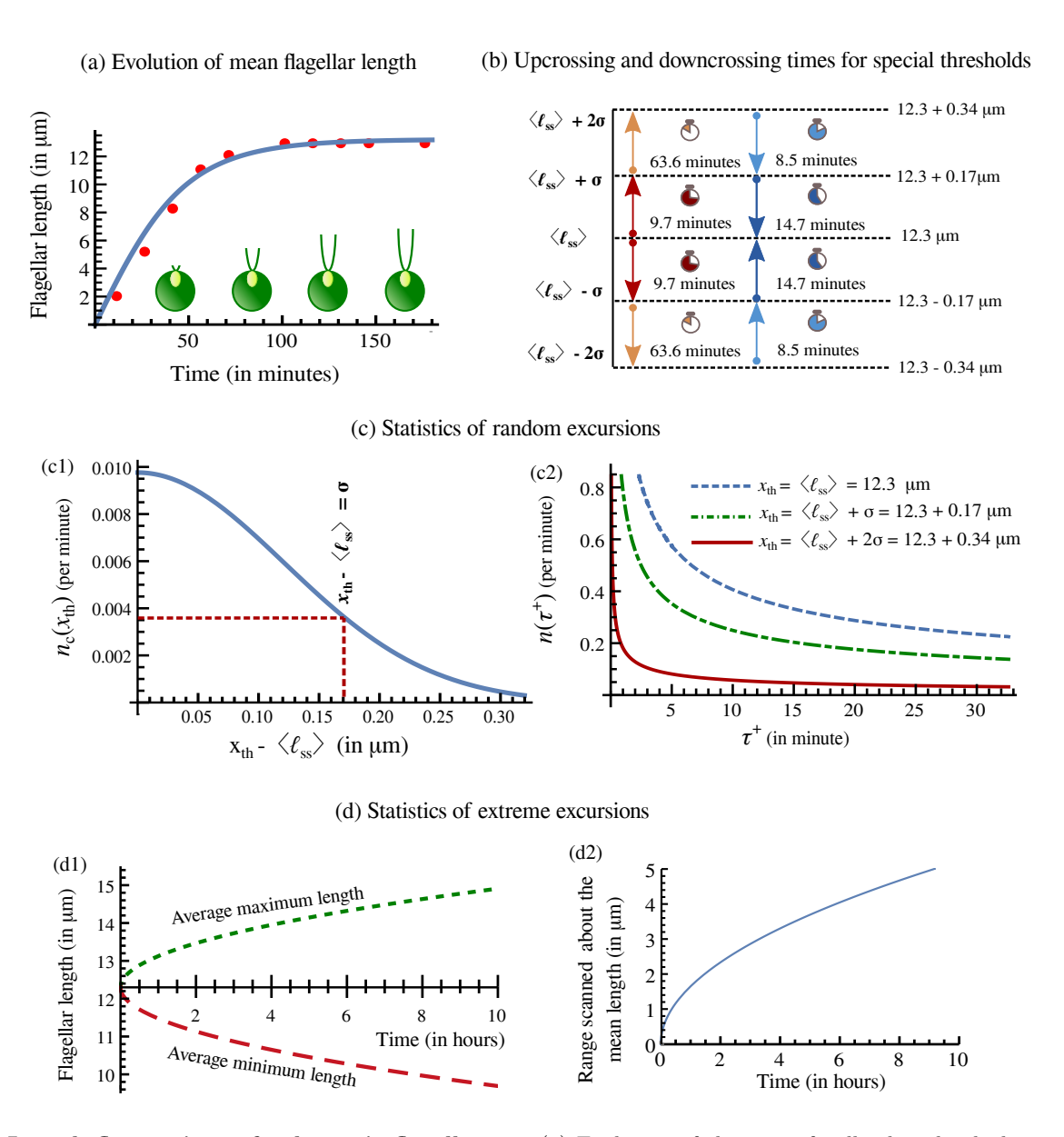


FIG. 9: Length fluctuations of eukaryotic flagellum: (a) Evolution of the mean fagellar length which we obtained by solving the rate equation 9 by using the values $A=809.6 \ min^{-1}$, $B=28.21 \ min^{-1}$ and C=0.0021. Line represents the theory and the dots are experimental data taken from Ishikawa and Marshall ([78])). The mean length in steady state is 12.3μ m. (b) Hitting times for special thresholds in flagellum. Levels are indicated by the horizontal. Tip of the arrows indicate the terminating point and their base (with a circle) indicate the initiating point. The mean upcrossing and downcrossing times are denoted besides these arrow which indicate the transition. (c) Statistics of random excursions. (c1) Number of upcrossings $n(x_{th})$ per unit minute as a function of threshold x_{th} . (c2) Number of sojourns per unit time above a given threshold (indicated along the lines) whose duration exceed τ^+ minutes. (d) Statistics of extreme excursions - (d1) Average maximum (denoted by dotted green line) and minimum flagellar length (dashed red line) about its mean length as a function of time. (d2) Average range scanned by the flagellar tip as a function of time. For (b-d), $\kappa=0.061 \ \text{min}^{-1}$ and $D=56.42 \ \text{min}^{-1}$

IX. SUMMARY AND CONCLUSION

In a classic essay, titled "on being the right size", J.B.S. Haldane [2] first analyzed the physical reasons that would explain why "for every type of animal there is a convenient size". Haldane focused his analysis on the size of whole organisms. The mechanisms that ensure the "convenient" size of a cell [7] and sub-cellular structures [5–7] have become a very active field of research in recent years.

There are three different kinds of questions that need to be addressed:

- (I) The relations between the size and various other parameters that characterize the structure or dynamics of the organism; these observations have been presented mostly in the form of scaling relations that are usually referred to allometric relations.
- (II) The allometric relations are explained in terms of constraints imposed by the laws of physics and chemistry; these are, for example, mechanical strength or chemical reaction rate, etc. Having understood the causes of selecting the specific convenient size, one also needs to understand functional consequences of any deviation from that convenient size caused, possibly, by mutations.
- (III) Having discovered the allometric laws satisfied by the size and the physico-chemical origin of these laws, the next question is how does an organism grow up to a given size, stop further growth and maintain it subsequently.

It is the type (III) questions that we have addressed in a recent paper [18]. However, instead of a multi-cellular organism or a single cell, we have considered the size of subcellular structures. Long protrusions and membrane-bound organelles, that appear as cell appendages, are prominent among the sub-cellular structures. Except for a few papers, including ref.[18], all the works on length control of cell protrusions so far have investigated the time-dependence of the mean lengths. Moreover, those have mostly assumed either length-dependent growth or length-dependent shrinkage of the respective protrusions.

Going beyond the mean length, in this paper we have investigated various aspects of the fluctuations of the lengths of the cell protrusions in the steady-state. Using the formalisms of stochastic processes, we have first mapped the time evolution of the tip of a dynamic protrusion on an Ornstein-Uhlenbeck process. The mapping is very general and is applicable for all the three classes of protrusions listed in Table I. Then, we derive analytical expressions for several statistical characteristics of the fluctuations using the techniques of level crossing pioneered by Rice [34], and pedagogically presented by Stratonovich [61], Brainina [32], Masoliver [46] and others. The results could be segregated into three groups and summarized in table II.

For a specific case study, we have considered eukaryotic fagellum (also called a cilium). We have first extracted

the rate parameters from the experimental data available in the literature. Then, plugging these rates into the analytical expressions that we have dereived in this paper,

Quantities	Symbol	Formula		
Statistics of passage times				
Mean exit time	$T_{\varepsilon}(x_U, x_L \underline{x_0, t_0})$	Equation (45)		
Mean upcrossing time	$T_{HU}(x_{th} \mid \underline{x_0}, \underline{t_0})$	Equation (49)		
Mean downcrossing time	$T_{HD}(x_{th} \mid \underline{x_{0}, \underline{t_0}})$	Equation (50)		
Statistics of random excursion				
Number density of upcrossings for the threshold x_{th}	n_c	Equation (70)		
Number density of sojourns above a threshold with sojourn time τ^+	$n(au^+)$	Equation (78) Equation (80)		
Distribution of sojourn time above a threshold x_{th}	$p_n(\tau^+)$	Equation (79) Equation (81)		
Statistics of extremal excursion				
Average maximum value attained about the mean position as a function of time .	$\langle x_{max}(t) 0\rangle$	Equation (86)		
Average maximum value attained about the mean position as a function of time.	$\langle x_{min}(t) 0\rangle$	Equation (88)		
Average range spanned about the mean position as a function of time .	$\langle x_{range}(t) 0\rangle$	Equation (89)		

TABLE II: List of important quantities derived in this paper which describe different aspects of level crossing for protrusions and filaments with fluctuating length.

we have plotted the statistical properties of the fluctuations of the lengths of the flagellum in the steady-state in Fig.9. As byproduct of this analysis we also get rough estimates of the typical length scales and time scales involved. Based on these estimates, we conclude that our predictions can be tested by analyzing a series of kymographs capturing the temporal evolution of length in wild type and mutant cells. We also believe that studies of fluctuations of the lengths of sensory cilia, in particular, will shed light on 'fading' of chemical signals just as Rice's pioneeing work on level crossing was motivated by fading of radio signals [34].

Acknowledgement : SP acknowledges support from IIT Kanpur through a teaching assistantship. D.C. acknowledges support from SERB (India) through a J.C. Bose National Fellowship.

Appendix A: Equivalence of Fokker-Planck and stochastic differential (Langevin) equation

The stochastic differential equation is

$$dy = R_{-}(y)dt + \frac{\sqrt{R_{+}(y)}}{\sqrt{N}}dW(t)$$
(A1)

Let f[y] be an arbitrary function of y. Expanding f[y] in second order:

$$df[y] = f[y+dy] - f[y]$$

$$= f[y] + f'[y]dy + \frac{1}{2}f''[y][dy]^2 - f[y]$$

$$= f'[y] \left(R_-(y)dt + \frac{\sqrt{R_+(y)}}{\sqrt{N}}dW(t)\right) + \frac{1}{2}f''[y] \left(R_-(y)dt + \frac{\sqrt{R_+(y)}}{\sqrt{N}}dW(t)\right)^2$$

$$Note: \text{ Neglecting the terms containing } (dt)^2 \text{ and } dtdW(t)$$

$$\simeq f'[y] \left(R_-(Y)dt + \frac{\sqrt{R_+(y)}}{\sqrt{N}}dW(t)\right) + \frac{1}{2}f''[y] \left(\frac{R_+(y)}{N}(dW(t))^2\right)$$

$$Note: \text{ Using the relation } (dW(t))^2 = dt$$

$$= \left(R_-(y)f'[y] + \frac{1}{2N}R_+(y)f''[y]\right)dt + \left(\frac{\sqrt{R_+(y)}}{\sqrt{N}}f[y]\right)dW(t) \tag{A2}$$

Let us consider the time development of the arbitrary function f[y(t)]. If we take the average of df[y] over realizations and divide by dt, we get

$$\frac{d\langle f[y]\rangle}{dt} = \frac{d}{dt} \left\langle \left(R_{-}(y)f'[y] + \frac{1}{2N} R_{+}(y)f''[y] \right) dt + \left(\frac{\sqrt{R_{+}(y)}}{\sqrt{N}} f[y] \right) dW(t) \right\rangle
= \left\langle R_{-}(y) \frac{\partial f[y]}{\partial y} + \frac{1}{2N} R_{+}(y) \frac{\partial^{2} f[y]}{\partial y^{2}} \right\rangle$$
(A3)

Now y evolves according to the conditional density $p(y, t|y_0, t_0)$. The left hand side of the above equation (A3) is simply given by

$$\frac{d\langle f[y]\rangle}{dt} = \frac{d}{dt} \int dY f(y) p(y, t|y_0, t_0) = \int dy f(y) \frac{\partial p(y, t|y_0, t_0)}{\partial t}$$
(A4)

(Because f(y) is not a function of t, therefore we can take it out. On the other hand, p(y,t) is a function of both y and t. Therefore, there will be a partial derivative. This is how Gardiner proceeds from here.)

Now going to the right hand side term of equation (A3)

$$\left\langle R_{-}(y)\frac{\partial f[y]}{\partial y} + \frac{1}{2N}R_{+}(y)\frac{\partial^{2} f[y]}{\partial y^{2}} \right\rangle = \int dy \left(R_{-}(y)\frac{\partial f[y]}{\partial y} + \frac{1}{2N}R_{+}(y)\frac{\partial^{2} f[y]}{\partial y^{2}} \right) p(y,t|y_{0},t_{0})
= \int dy f[y] \left(-\frac{\partial R_{-}(y)p(y,t|y_{0},t_{0})}{\partial y} + \frac{1}{2N}\frac{\partial^{2} R_{+}(y)p(y,t|y_{0},t_{0})}{\partial y^{2}} \right) \tag{A5}$$

Equating the last expressions of equation (A4) and (A5) we get

$$\int dY f(y) \frac{\partial p(y, t|y_0, t_0)}{\partial t} = \int dY f[y] \left(-\frac{\partial R_-(y)p(y, t|y_0, t_0)}{\partial y} + \frac{1}{2N} \frac{\partial^2 R_+(y)p(y, t|y_0, t_0)}{\partial y^2} \right). \tag{A6}$$

As f[y] is arbitrary, we can simply write the following

$$\frac{\partial p(y,t|y_0,t_0)}{\partial t} = -\frac{\partial R_-(y(t))p(Y,t|y_0,t_0)}{\partial y} + \frac{1}{2N} \frac{\partial^2 R_+(y(t))p(Y,t|y_0,t_0)}{\partial y^2}$$
(A7)

Therefore, we can say that for the following SDE

$$dy = R_{-}(y)dt + \frac{\sqrt{R_{+}(y)}}{\sqrt{N}}dW(t)$$
(A8)

the corresponding Fokker-Planck equation is given by

$$\frac{\partial p(y,t)}{\partial t} = -\frac{\partial R_{-}(y)p(y,t)}{\partial y} + \frac{1}{2N} \frac{\partial^{2} R_{+}(y)p(y,t)}{\partial y^{2}}$$
(A9)

and vice versa.

Appendix B: Mapping into Ornstein-Uhlenbeck procees

We have

$$y - y^* = \frac{x}{\sqrt{N}} \Rightarrow y = y^* + \frac{x}{\sqrt{N}}$$
 (B1)

Substituting this in equation (11) we get

$$d(y^* + \frac{x}{\sqrt{N}}) = R_-(y^* + \frac{x}{\sqrt{N}})dt + \frac{1}{\sqrt{N}}\sqrt{R_+(y^* + \frac{x}{\sqrt{N}})}dW(t)$$

$$\Rightarrow \frac{dx}{\sqrt{N}} = \left(R_-(y^*) + \frac{x}{\sqrt{N}}R'_+(y^*)\right)dt + \frac{1}{\sqrt{N}}\sqrt{\left(R_+(y^*) + \frac{x}{\sqrt{N}}R'_+(y^*)\right)}dW(t)$$
(B2)

Using the defination of $R_{-}(y)$ (equation (6)) and equation (10), we get $R_{-}(y^{*}) = 0$. Neglecting the term $R'_{+}(y^{*})$ inside the square root we get

$$\Rightarrow \frac{dx}{\sqrt{N}} = \frac{x}{\sqrt{N}} R'_{+}(y^*) dt + \frac{1}{\sqrt{N}} \sqrt{R_{+}(y^*)} dW(t)$$

$$\Rightarrow dx = R'_{+}(y^*) x dt + \sqrt{R_{+}(y^*)} dW(t)$$
(B3)

which is the transformed stochastic differential equation (13) we wanted to derive from equation (11).

Appendix C: Statistics of passage times

Mean exit time

The escape probability $\mathcal{E}(t; x_U, x_L | \underline{x_0, t_0})$ is introduced in equation (39). For our convinience, we denote it simply by $\mathcal{E}(x_0, t)$. Integrating the backward FPE (38) with respect to final position x (as done while defining the escape probability in equation (38)) it can be checked that the escape probability $\mathcal{E}(x_0, t)$ obeys the backward FPE i.e,

$$\frac{\partial \mathcal{E}(x_0, t)}{\partial t} = -\kappa x_0 \frac{\partial [\mathcal{E}(x_0, t)]}{\partial x_0} + \frac{D}{2} \frac{\partial^2 \mathcal{E}(x_0, t)}{\partial x_0^2}$$
(C1)

subjected to the initial condition

$$\mathcal{E}(x_0, t_0) = 0 \tag{C2}$$

and the following boundary conditions

$$\mathcal{E}(x_U, t) = 1 \text{ and } \mathcal{E}(x_L, t) = 1$$
 (C3)

The initial condition (equation (C2)) indicates that initially x_0 lies between x_U and x_L and the boundary condition (equation (C3)) indicates whenever the length hits either of the thresholds, it successfully exits the zone.

Using the Laplace transform

$$\tilde{\mathcal{E}}(x_0, s) = \int_0^\infty e^{-st} \mathcal{E}(x_0, t) dt$$
 (C4)

the backward FPE (equation (C1)) gets converted to an ordinary differential equation

$$-\kappa x_0 \frac{d\tilde{\mathcal{E}}(x_0, s)}{dx_0} + \frac{D}{2} \frac{d^2 \tilde{\mathcal{E}}(x_0, s)}{dx_0^2} = s\tilde{\mathcal{E}}(x_0, s) - 1 \quad (C5)$$

with boundary conditions

$$\tilde{\mathcal{E}}(x_L, s) = \tilde{\mathcal{E}}(x_U, s) = 1/s$$
 (C6)

Now onwards, for our convinience, we will denote the corresponding $pdf \ p_{\mathcal{E}}(t, x_U, x_L | \underline{x_0, t_0})$ by a simpler notation $p_{\mathcal{E}}(x_0, t)$. The moments of the exit time are given by

$$\mathcal{T}_{\mathcal{E}}^{n}(x_{U}, x_{L} | \underline{x_{0}, t_{0}}) = \int_{0}^{\infty} t^{n} p_{\mathcal{E}}(x_{0}, t) dt \qquad (C7)$$

where the zeroth moment corresponding to n=0 is $\mathcal{T}^0_{\mathcal{E}}=1$ and the first moment corresponding to n=1 is the mean exit time $\mathcal{T}_{\mathcal{E}}(x_U,x_L|\underline{x_0,t_0})$. Let us denote the moments of exit time $\mathcal{T}^n_{\mathcal{E}}(x_U,x_L|\underline{x_0,t_0})$ simply by $\mathcal{T}^n_{\mathcal{E}}(x_0)$. If $\tilde{p}_{\mathcal{E}}(x_0,s)$ is the Laplace transform of the pdf $p_{\mathcal{E}}(x,t)$, the moments of escape time are given by

$$\mathcal{T}_{\mathcal{E}}^{n}(x_0) = (-1)^n \frac{\partial^n}{\partial s^n} \tilde{p}_{\mathcal{E}}(x_0, s) \bigg|_{s=0}$$
 (C8)

Therefore, $\tilde{p}_{\mathcal{E}}(x_0, s)$ can be expanded and its series form is given by the Laplace transform $\tilde{p}_{\mathcal{E}}(x_0, s)$ can be written as a power series of the Laplace variable s

$$\tilde{p}_{\mathcal{E}}(x_0, s) = \sum_{n=0}^{\infty} \frac{(-1)^n}{n!} \mathcal{T}_{\mathcal{E}}^n(x_0) s^n$$
 (C9)

provided all the moments of the escape time exists.

 $p_{\mathcal{E}}(x_0, t)$ is obtained from the probability $\mathcal{E}(x_0, t)$ by taking derivate with respect to t

$$p_{\mathcal{E}}(x_0, t) = \frac{\partial \mathcal{E}(x_0, t)}{\partial t}$$
 (C10)

Taking into account the fact that $\mathcal{E}(x_0, 0) = 0$ which indicates that initially it is impossible to escape the safe zone, it can be shown that the relation between the Laplace transforms $\tilde{\mathcal{E}}(x_0, s)$ and $\tilde{p}_{\mathcal{E}}(x_0, s)$ is

$$\tilde{p}_{\mathcal{E}}(x_0, s) = s \ \tilde{\mathcal{E}}(x_0, s)$$
 (C11)

which is obtained by taking the Laplace transforms of the terms on both side of the equation (C10). From equation

(C9) and(C11), we can see that the

$$\tilde{\mathcal{E}}(x_0, s) = \frac{1}{s} \sum_{n=0}^{\infty} \frac{(-1)^n}{n!} \mathcal{T}_{\mathcal{E}}^n(x_0) s^n$$

$$= \frac{1}{s} \left(1 - s \mathcal{T}_{\mathcal{E}}(x_0) + \sum_{n=2}^{\infty} \frac{(-1)^n}{n!} \mathcal{T}_{\mathcal{E}}^n(x_0) s^n \right) \quad (C12)$$

On rearranging the above equation

$$\frac{1}{s} - \tilde{\mathcal{E}}(x_0, s) = \mathcal{T}_{\mathcal{E}}(x_0) - \sum_{n=2}^{\infty} \frac{(-1)^n}{n!} \mathcal{T}_{\mathcal{E}}^n(x_0) s^{n-1}$$
(C13)

and taking the limit $s \to 0$ we get

$$\lim_{s \to 0} \left[\frac{1}{s} - \tilde{\mathcal{E}}(x_0, s) \right] = \mathcal{T}_{\mathcal{E}}(x_0) . \tag{C14}$$

Plugging this relation mentioned in equation (C14) into the backward Fokker-Planck equation (C1), we get

$$\lim_{s \to 0} \left\{ -\kappa x_0 \frac{d}{dx_0} \left[\frac{1}{s} - \mathcal{T}_{\mathcal{E}}(x_0) \right] + \frac{D}{2} \frac{d^2}{dx_0^2} \left[\frac{1}{s} - \mathcal{T}_{\mathcal{E}}(x_0) \right] \right\} = \lim_{s \to 0} \left\{ s \left[\frac{1}{s} - \mathcal{T}_{\mathcal{E}}(x_0) \right] - 1 \right\}$$
(C15)

which simplifies to

$$-\kappa x_0 \frac{d\mathcal{T}_{\mathcal{E}}(x_0)}{dx_0} + \frac{D}{2} \frac{d^2 \mathcal{T}_{\mathcal{E}}(x_0)}{dx_0^2} = -1.$$
 (C16)

On rearranging the corresponding boundary condition (C6) and taking limits

$$\lim_{s \to 0} \left[\frac{1}{s} - \tilde{\mathcal{E}}(x_U) \right] = \lim_{s \to 0} \left[\frac{1}{s} - \tilde{\mathcal{E}}(x_L) \right] = 0$$
 (C17)

we get the boundary condition

$$\mathcal{T}_{\mathcal{E}}(x_U) = \mathcal{T}_{\mathcal{E}}(x_L) = 0.$$
 (C18)

for the ordinary differential equation (C16).

2. Mean hitting time

By integrating the backward FPE (38) with respect to the final position and using the defination of hitting probability given in equation (40) or (41), we can show that $\mathcal{H}(t; x_{th}|x_0, t_0)$ (simply written as $\mathcal{H}(x_0, t)$) obeys the backward $\overline{\text{FPE}}$:

$$\frac{\partial \mathcal{H}(x_0, t)}{\partial t} = -\kappa x \frac{\partial \mathcal{H}(x_0, t)}{\partial x_0} + \frac{D}{2} \frac{\partial^2 \mathcal{H}(x_0, t)}{\partial x_0^2} \quad (C19)$$

with initial condition

$$\mathcal{H}_{\ell}(x_0, 0) = 0 \tag{C20}$$

and boundary condition given by

$$\mathcal{H}(x_{th}, t) = 1. \tag{C21}$$

We rescale t by multiplying it with κ . So, replacing the t with the rescaled time t_r which is given by

$$t_r = \kappa t$$
 . (C22)

we transform the partial differential equation

$$\frac{\partial \mathcal{H}(x_0, t_r)}{\partial t^r} = -x \frac{\partial \mathcal{H}(x_0, t_r)}{\partial x_0} + \frac{D}{2\kappa} \frac{\partial^2 \mathcal{H}(x_0, t_r)}{\partial x_0^2} \quad (C23)$$

The laplace transform of the hitting probability is given by

$$\tilde{\mathcal{H}}(x_0, s) = \int_0^\infty e^{-st_r} \mathcal{H}(x_0, t_r) dt_r \qquad (C24)$$

and using this Laplace transform, we convert the partial differential equation (equation (C23)) into an ordinary differential equation given by

$$-x\frac{d\tilde{\mathcal{H}}(x_0,s)}{dx} + \frac{D}{2\kappa}\frac{d^2\tilde{\mathcal{H}}(x_0,s)}{dx^2} = s\tilde{\mathcal{H}}(x_0,s) \quad (C25)$$

which is subjected to the boundary condition

$$\tilde{\mathcal{H}}(x_{th}, s) = \frac{1}{s} . \tag{C26}$$

Using the change of variables

$$z = \frac{\kappa}{D}x_0^2 \tag{C27}$$

one can check that equation (C25) can be recasted to the following second order ODE

$$z\frac{d^2\tilde{\mathcal{H}}(z,s)}{dz^2} + \left(\frac{1}{2} - z\right)\frac{d\tilde{\mathcal{H}}(z,s)}{dz} - \frac{s}{2}\tilde{\mathcal{H}}(z,s) = 0 \quad (C28)$$

whose general solution is a linear combination of Kummer functions. Hence the general solution of the equation (C25) is given by

$$\tilde{\mathcal{H}}(x_0, s) = C_1 F(s/2, 1/2, \kappa x_0^2/D) + C_2 U(s/2, 1/2, \kappa x_0^2/D)$$
 (C29)

Now let us have a look at the asymptotic behaviour of the Kummer functions. In the limit $x_0 \to \pm \infty$

$$\lim_{x_0 \to \pm \infty} F(s/2, 1/2, \kappa x_0^2/D) =$$

$$= \frac{\Gamma(1/2)}{\Gamma(s/2)} x_0^{s-1} e^{\kappa x_0^2/D} [1 + \mathcal{O}(1/x_0^2)] \to \infty \qquad (C30)$$

so, it can serve to be the solution when x_0 is bounded i.e, $x_0^2 < x_{th}^2$. On the other hand,

$$\lim_{x_0 \to \pm \infty} U(s/2, 1/2, \kappa x_0^2/D) = |x_0|^{-s} [1 + \mathcal{O}(1/x_0^2)] \to 0$$
(C31)

and this indicates that it can serve as the solution when x_0 remains unbounded, i.e, $x_0^2 > x_{th}^2$.

 C_1 and C_2 can be evaluated using the boundary condition given by equation (C26) and collectively, the unique solution of equation (C25) is given by

$$\tilde{\mathcal{H}}(x_0, s) = \begin{cases}
\frac{F(s/2, 1/2, \kappa x_0^2/D)}{sF(s/2, 1/2, \kappa x_{th}^2/D)} & \text{when } |x_0| < |x_{th}| \\
\frac{U(s/2, 1/2, \kappa x_{th}^2/D)}{sU(s/2, 1/2, \kappa x_{th}^2/D)} & \text{when } |x_0| > |x_{th}|
\end{cases}$$
(C32)

Using the arguments used to derive the relation stated in equation (C14), we can arrive at the following

$$\mathcal{T}_{\mathcal{H}}^{r}(x_{th}|\underline{x_0, t_0}) = \lim_{s \to 0} \left[\frac{1}{s} - \tilde{\mathcal{H}}(x_0) \right]$$
 (C33)

where $\mathcal{T}_{\mathcal{H}}^r(x_{th}|\underline{x_0,t_0})$ (simply denoted by $\mathcal{T}_{\mathcal{H}}^r(x_0)$) is the rescaled mean hitting time.

For $x_0 < x_{th}$, the rescaled mean hitting (upcrossing) time $\mathcal{T}_{\mathcal{H}U}^r(x_0)$ for hitting the threshold is

$$\mathcal{T}_{\mathcal{H}}^{r}(x_0) = \mathcal{T}_{\mathcal{H}\mathcal{U}}^{r}(x_0) = \lim_{s \to 0} \left[\frac{1}{s} - \frac{F(s/2, 1/2, \kappa x_0^2/D)}{sF(s/2, 1/2, \kappa x_{th}^2/D)} \right]. \tag{C34}$$

Plugging the following relation in the above equation

$$F(s/2, 1/2, \kappa x^2/D)$$

$$= 1 + s \int_0^{\kappa x^2/D} F(1, 3/2, z) dz + \mathcal{O}[s^2] \qquad (C35)$$

we get

$$\mathcal{T}_{\mathcal{H}\mathcal{U}}(x_0) = \frac{1}{\kappa} \mathcal{T}_{\mathcal{H}\mathcal{U}}^r(x_0) = \frac{1}{\kappa} \int_{\kappa x_0^2/D}^{\kappa x_{th}^2/D} F(1, 3/2, z) dz$$
$$= \frac{\sqrt{\pi}}{\kappa} \int_{\sqrt{\kappa}|x_{th}|/\sqrt{D}}^{\sqrt{\kappa}|x_{th}|/\sqrt{D}} e^{y^2} \operatorname{erf}(y) dy \qquad (C36)$$

For $x > x_{th}$, the rescaled mean hitting (downcrossing) $\mathcal{T}_{HD}^{r}(x_0)$ time for hitting the threshold is

$$\mathcal{T}_{\mathcal{H}}^{r}(x_0) = \mathcal{T}_{\mathcal{H}\mathcal{D}}^{r}(x_0) = \lim_{s \to 0} \left[\frac{1}{s} - \frac{U(s/2, 1/2, \kappa x_0^2/D)}{sU(s/2, 1/2, \kappa x_{th}^2/D)} \right]. \tag{C37}$$

Plugging the following relation in the above equation

$$U(s/2, 1/2, \kappa x^2/D) = 1 - \frac{s}{2} \left[\psi(1/2) + \int_0^{\kappa x^2/D} U(1, 3/2, z) dz + \mathcal{O}[s^2] \right]$$
 (C38)

we get

$$\mathcal{T}_{\mathcal{H}\mathcal{D}}(x_0) = \frac{1}{\kappa} \mathcal{T}_{\mathcal{H}\mathcal{D}}^r(x_0) = \frac{1}{2\kappa} \int_{\kappa x_{th}^2/D}^{\kappa x_0^2/D} U(1, 3/2, z) dz$$
$$= \frac{\sqrt{\pi}}{\kappa} \int_{\sqrt{\kappa}|x_0|/\sqrt{D}}^{\sqrt{\kappa}|x_0|/\sqrt{D}} e^{y^2} \operatorname{erfc}(y) dy \qquad (C39)$$

Appendix D: Statistics of random excursions

1. Mean density of crossing a threshold

Here we perform the integration in equation (70) to get the expression of mean density of upcrossings which we directly wrote in equation (71).

The steady state distribution of protrusion length (X(t)) is a Gaussian distribution

$$\frac{1}{\sigma_x \sqrt{2\pi}} e^{-x^2/(2\sigma_x^2)} \tag{D1}$$

with mean μ_x given by

$$\mu_x = x^* = 0 \tag{D2}$$

and standard deviation σ_x given by

$$\sigma_x = \sqrt{\frac{D}{2\kappa}} \tag{D3}$$

Since x follows a Gaussian distribution, then its derivative \dot{x} also obeys a Gaussian distribution with mean $\mu_{\dot{x}}=0$ and standard deviation $\sigma_{\dot{x}}$ given by

$$\sigma_{\dot{x}}^2 = -\mathcal{C}''(\tau)|_{\tau=0} = -\frac{d}{d\tau} \left(-\frac{D}{2\kappa} e^{-\kappa\tau} \right)_{\tau=0} = D\kappa \quad (D4)$$

For integrating the expression in equation (70), we use the following result

$$\int_{0}^{\infty} \dot{x}p(\dot{x}) \ d\dot{x} = \int_{0}^{\infty} \dot{x} \frac{1}{\sigma_{\dot{x}}\sqrt{2\pi}} e^{-\dot{x}^{2}/(2\sigma_{\dot{x}}^{2})} d\dot{x} = \frac{\sigma_{\dot{x}}}{\sqrt{2\pi}}.$$
(D5)

Using this, we get the expression for mean density $n_c(x_{th})$ as

$$n_c(x_{th}) = p_{ss}(x_{th}) \int_0^\infty \dot{x} p(\dot{x}) d\dot{x}$$

= $\frac{1}{2\pi} \frac{\sigma_{\dot{x}}}{\sigma_x} e^{-x^2/(2\sigma_x^2)} = \frac{\kappa}{2\pi} e^{-\kappa x_{th}^2/D}$ (D6)

2. Statistics of sojourns above a threhold

For obtaining the expression for $n(\tau^+)$, we need the expression for $p^+(x,t)$ and the following limit

$$\lim_{t \to 0} \frac{p^+(x,t)}{\Delta t} \tag{D7}$$

For convenience , let us introduce the following function $w^+(x,t)$

$$w^{+}(x,t) = \frac{1}{p_{st}(x)} \lim_{t \to 0} \frac{p^{+}(x,t)}{\Delta t}$$
 (D8)

Just as $p^+(x,t)$ satisfies the Fokker-Planck equation (72), this new function $w^+(x,t)$ also satisfies the following Fokker-Planck equation

$$\frac{\partial w^{+}(x,t)}{\partial t} = \frac{\partial}{\partial x} \left[\kappa x \ w^{+}(x,t) \right] + \frac{D}{2} \frac{\partial^{2} w^{+}(x,t)}{\partial x^{2}}$$
 (D9)

and from the initial and boundary conditions (equation (73) and (74) respectively) we can infer that the FPE (equation (D9)) is subjected to the following conditions

$$w^{+}(x,t) = 0 \text{ for } t < 0,$$

 $w^{+}(x_{th},t) = \delta(t).$ (D10)

In terms of $w^+(x,t)$, $n(\tau^+)$ is given by

$$n(\tau^+) = p_{st} \int_{x_{th}}^{\infty} w^+(x, \tau) dx$$
 (D11)

The partial differential equation (D9) will be solved by using the Carlson-Laplace transform. The transform of $w^+(x,t)$ is given by

$$\tilde{w}^{+}(x,s) = s \int_{0}^{\infty} e^{-st} w^{+}(x,t)dt$$
 (D12)

The Fokker-Planck equation (D9) in terms of $\tilde{w}^+(x,s)$ is

$$s\tilde{w}^{+}(x,s) = \frac{\partial}{\partial x} \left[\kappa x \ \tilde{w}^{+}(x,s) \right] + \frac{D}{2} \frac{\partial^{2} \tilde{w}^{+}(x,s)}{\partial x^{2}}$$
 (D13)

and the boundary condition takes the form

$$\tilde{w}^+(x_{th}, s) = s \tag{D14}$$

Using this boundary condition and the fact that the corresponding flux vanishes as $x \to \infty$, the Fokker-Planck equation (D13) can be integrated to

$$\int_{x_{th}}^{\infty} \tilde{w}^{+}(x,s)dx = -\frac{1}{s} \left[\frac{D}{2} \frac{\partial \tilde{w}^{+}(x_{th},s)}{\partial x} + \kappa x_{th} \, \tilde{w}^{+}(x_{th},s) \right]$$
(D15)

Rearranging Eq.(D13), we get

$$\frac{\partial^2 \tilde{w}^+(x,s)}{\partial x^2} + \left(\frac{2\kappa}{D}\right) x \frac{\partial \tilde{w}^+(x,s)}{\partial x} + \left(\frac{2\kappa}{D}\right) \left(1 - \frac{s}{\kappa}\right) \tilde{w}^+(x,s) = 0$$
(D16)

which, upon change of variable from x to z defined by

$$z = \sqrt{\frac{2\kappa}{D}}x,\tag{D17}$$

gets transformed to

$$\frac{\partial^2 \tilde{w}^+(z,s)}{\partial z^2} + z \frac{\partial \tilde{w}^+(z,s)}{\partial z} + \left(1 - \frac{s}{\kappa}\right) \tilde{w}^+(z,s) = 0. \text{ (D18)}$$

The general solution for the above equation has the form

$$\tilde{w}^{+}(x,s) = C_1 e^{-z^2/4} \mathcal{D}_{-s/k}(z) + C_2 e^{-z^2/4} \mathcal{D}_{-s/k}(-z)$$
(D19)

where $\mathcal{D}_{-s/k}(y)$ is the parabolic cylindrical function and C_1 and C_2 are arbitrary constants fixed by the boundary conditions. As the first term vanishes as $z \to \infty$ whereas the second does not, it qualifies as the physically allowed solution. Imposing the boundary condition (D14) at $x = x_{th}$ we get

$$\tilde{w}^{+}(x_{th}, s) = s = C_1 e^{-(\kappa x_{th}^2)/(2D)} \mathcal{D}_{-s/k} \left(\sqrt{\frac{2\kappa}{D}} x_{th} \right)$$
(D20)

which gives the expression for C_1 that we use to write the solution

$$\tilde{w}^{+}(x,s) = s \exp\left(\frac{x_{th}^{2} - x^{2}}{2D}\right) \frac{\mathcal{D}_{-s/k}(\sqrt{\frac{2\kappa}{D}}x)}{\mathcal{D}_{-s/k}(\sqrt{\frac{2\kappa}{D}}x_{th})}$$
(D21)

The Carlson-Laplace transform of $n(\tau)$ is denoted by $\tilde{n}(s)$ and the expression of $\tilde{n}(s)$ using equation (D8), (D11) and (D15), we get

$$\tilde{n}(s) = -\frac{p_{st}(x)}{s} \left[\frac{D}{2} \frac{\partial \tilde{w}^+(x_{th}, s)}{\partial x} + \kappa x_{th} \ \tilde{w}^+(x_{th}, s) \right]$$
(D22)

Substituting the expression for $\tilde{w}^+(x,s)$ in equation (D22) and after some rearrangement we get

$$\tilde{n}(x,s) = -p_{st}(x_{th})$$

$$\times \left[\frac{D}{2D_{-s/k}(\sqrt{\frac{2\kappa}{D}})x_{th}} \exp\left(\frac{\kappa(x_{th}^2 - x_{th}^2)}{2D}\right) \left(\sqrt{\frac{2\kappa}{D}}\right) \left\{ -\frac{1}{2}\sqrt{\frac{2\kappa}{D}}\mathcal{D}_{-s/k}\left(\sqrt{\frac{2\kappa}{D}}x_{th}\right) + \mathcal{D}'_{-s/k}\left(\sqrt{\frac{2\kappa}{D}}x_{th}\right) \right\} + \kappa x_{th} \right]$$

$$(Using the identity $\mathcal{D}'_{\nu}(z) - \frac{z}{2}\mathcal{D}_{\nu}(z) + \mathcal{D}_{\nu+1}(z) = 0)$

$$= -p_{st}(x_{th}) \left[\frac{D}{2D_{-s/k}(\sqrt{\frac{2\kappa}{D}})x_{th}} \left(\sqrt{\frac{2\kappa}{D}}\right) \left\{ -\mathcal{D}_{-s/k+1}\left(\sqrt{\frac{2\kappa}{D}}x_{th}\right) \right\} + \kappa x_{th} \right]$$

$$(Using the identity $\mathcal{D}_{\nu+1}(z) - z\mathcal{D}_{\nu}(z) + \nu\mathcal{D}_{\nu-1}(z) = 0)$

$$= -p_{st}(x_{th}) \left[\frac{D}{2D_{-s/k}(\sqrt{\frac{2\kappa}{D}})x_{th}} \left(\sqrt{\frac{2\kappa}{D}}\right) \left\{ -\left(\sqrt{\frac{2\kappa}{D}}x_{th}\right)\mathcal{D}_{-s/k}\left(\sqrt{\frac{2\kappa}{D}}x_{th}\right) + (-s/k)\mathcal{D}_{-s/k-1}\left(\sqrt{\frac{2\kappa}{D}}x_{th}\right) \right\} + \kappa x_{th} \right]$$

$$= -p_{st}(x_{th}) \left[-s\sqrt{\frac{D}{2\kappa}} \frac{\mathcal{D}_{-s/k-1}\left(\sqrt{\frac{2\kappa}{D}}x_{th}\right)}{\mathcal{D}_{-s/k}\left(\sqrt{\frac{2\kappa}{D}}x_{th}\right)} \right] = s\sqrt{\frac{D}{2\kappa}} p_{st}(x_{th}) \frac{\mathcal{D}_{-s/k-1}\left(\sqrt{\frac{2\kappa}{D}}x_{th}\right)}{\mathcal{D}_{-s/k}\left(\sqrt{\frac{2\kappa}{D}}x_{th}\right)}$$

$$(D23)$$$$$$

a. Special threshold $x_{th} = 0$

One particular case of interest is $x_{th} = 0$. Substituting $x_{th} = 0$ in equation (D23), we get

$$\tilde{n}(x,s) = s \sqrt{\frac{D}{2\kappa}} p_{st}(0) \frac{\mathcal{D}_{-s/k-1}(0)}{\mathcal{D}_{-s/k}(0)}$$
 (D24)

Using the identity

$$\mathcal{D}_{\nu}(0) = \sqrt{\frac{\pi}{2^{\nu}}} \frac{1}{\Gamma\left(\frac{\nu+1}{2}\right)}$$
 (D25)

the expression in equation (D24) simplifies to

$$\tilde{n}(x,s) = s \sqrt{\frac{D}{2\kappa}} \frac{p_{st}(0)}{\sqrt{2}} \frac{\Gamma(\frac{1}{2} + \frac{s}{2\kappa})}{\Gamma(1 + \frac{s}{2\kappa})}$$
(D26)

Using the defination of Beta function

$$\mathcal{B}(a,b) = \frac{\Gamma(a)\Gamma(b)}{\Gamma(a+b)}$$
 (D27)

and indentifying $a=1/2+s/(2\kappa)$ and b=1/2 , equation (D26) takes the form

$$\tilde{n}(x,s) = s \sqrt{\frac{D}{2\kappa}} \frac{p_{st}(0)}{\sqrt{2}} \frac{\mathcal{B}(s/(2\kappa), 1/2)}{\Gamma(1/2)}$$
 (D28)

The inverse Carlson-Laplace transform of the above expression is straight forward and we get

$$n(\tau) = p_{st}(0) \sqrt{\frac{D\kappa}{\pi}} \frac{1}{\sqrt{e^{2\kappa\tau} - 1}}$$
 (D29)

b. Rarely visited thresholds

In case of higher thresholds $(x_{th} >> D/2\kappa)$, the drift that acts on the Brownian particle which makes shorter excursion beyond the threshold x_{th} can be approximated as a $\kappa x \approx \kappa x_{th}$. So the equation (D16) simplifies to

$$s\tilde{w}^{+}(x,s) = \kappa x_{th} \frac{\partial \tilde{w}^{+}(x,s)}{\partial x} + \frac{D}{2} \frac{\partial^{2} \tilde{w}^{+}(x,s)}{\partial x^{2}}$$
(D30)

whose general solution is

$$\tilde{w}^{+}(x,s) = C_1 \exp\left(-\frac{x}{D}(\kappa x_{th} + \sqrt{(\kappa x_{th})^2 + 2sD})\right) + C_2 \exp\left(-\frac{x}{D}(\kappa x_{th} - \sqrt{(\kappa x_{th})^2 + 2sD})\right)$$
(D31)

Using the boundary condition (equation D14), we get

$$\tilde{w}^{+}(x,s) = s \times \exp\left(\frac{(x_{th} - x)}{D}(\kappa x_{th} - \sqrt{(\kappa x_{th})^{2} + 2sD})\right) \quad (D32)$$

Using it in equation (D24), we get

$$\tilde{n}(s) = p_{st}(x) \frac{sD}{\kappa x_{th} + \sqrt{(\kappa x_{th})^2 + 2sD}}$$
 (D33)

The inverse Carlson-Laplace transform is given by

$$n(\tau) = \frac{p_{st}(x_{th})}{2} \left[\frac{1}{\sqrt{\pi \tau/2D}} e^{-(\kappa x_{th})^2 \tau/(2D)} - (\kappa x_{th}) \operatorname{erfc} \left(\kappa x_{th} \sqrt{\frac{\tau}{2D}} \right) \right]$$
(D34)

Appendix E: Extremal excursions

The $pdf p_{max}(t; \zeta | x_0, t_0)$ is given by

$$p_{max}(t;\zeta|\underline{x_0,t_0}) = \frac{\partial \mathcal{M}_{max}(t;\zeta|\underline{x_0,t_0})}{\partial \zeta}$$
$$= -\frac{\partial \mathcal{H}_U(t;\zeta|\underline{x_0,t_0})}{\partial \zeta}\Theta(\zeta - x_0)$$
(E1)

where we have used (84) in the second step. Therefore,

$$\langle x_{max}(t)|x_0\rangle = \int_{-\infty}^{\infty} \zeta \ p_{max}(t;\zeta|\underline{x_0,t_0}) \ d\zeta$$
$$= x_0 + \int_{x_0}^{\infty} \mathcal{H}_U(t;\zeta|\underline{x_0,t_0}) d\zeta$$
(E2)

For $x_0 = 0$, from the above equation we get

$$\langle x_{max}(t)|0\rangle = \int_0^\infty \mathcal{H}_U(t;\zeta|\underline{0,t_0})d\zeta$$
 (E3)

In the above equation, replacing the time variable t with the rescaled time variable t_r where $t_r = \kappa t$, we get

$$\langle x_{max}(t_r)|0\rangle = \int_0^\infty \mathcal{H}_U(t_r;\zeta|\underline{0,t_{r0}})d\zeta \tag{E4}$$

Taking the the Laplace transform of both the sides

$$\langle \tilde{x}_{max}(s)|0\rangle = \int_0^\infty \tilde{\mathcal{H}}_U(s;\zeta|\underline{0}) \ d\zeta$$
$$= \frac{1}{s} \int_0^\infty \frac{F(s/2,1/2,0)}{F(s/2,1/2,\kappa\zeta^2/D)} \ d\zeta \tag{E5}$$

where we have used the expression of $\tilde{\mathcal{H}}_U(s;\zeta|\underline{0})$ which was already derived in appendix C2 and given in equation (C32). Using the following value,

$$F(s/2, 1/2, 0) = 0 (E6)$$

and using the following expansion

$$F(s/2, 1/2, \kappa \zeta^2/D) = 1 + s \frac{\kappa \zeta^2}{D}$$
 (E7)

for small ζ the integral in equation (E5) simplifies to

$$\langle \tilde{x}_{max}(s)|0\rangle = \frac{1}{s} \int_0^\infty \frac{d\zeta}{1 + (s\kappa\zeta^2/D)} = \frac{\pi}{2} \sqrt{\frac{D}{\kappa}} s^{-3/2}$$
(E8)

Carrying out the inverse Laplace transform we get

$$\langle x_{max}(t_r)|0\rangle = \left(\pi \frac{D}{\kappa} t_r\right)^{1/2}.$$
 (E9)

Finally, resatoring physical time t, i.e., replacing t_r by κt , we get

$$\langle x_{max}(t)|0\rangle = \sqrt{\pi Dt}$$
 (E10)

Alberts, Bruce. Molecular Biology of the Cell. Garland Science, 2008.

^[2] J.B.S. Haldane, On being the right size, Harper's magazine (March, 1926).

^[3] J. T. Bonner, Why Size matters: From Bacteria to Blue Whales (Princeton University Press, 2006).

^[4] Hamant O, Saunders TE. Shaping Organs: Shared Structural Principles Across Kingdoms [published online ahead of print, 2020 Jul 6]. Annu Rev Cell Dev Biol. 2020;10.1146/annurev-cellbio-012820-103850. doi:10.1146/annurev-cellbio-012820-103850

^[5] Marshall, Wallace F. How Cells Measure Length on Sub-

- cellular Scales. Trends in cell biology vol. 25,12 (2015): 760-768. doi:10.1016/j.tcb.2015.08.008
- [6] Marshall, Wallace F. Subcellular size. Cold Spring Harbor perspectives in biology vol. 7,6 a019059. 8 May. 2015, doi:10.1101/cshperspect.a019059
- [7] Marshall, Wallace F. Cell Geometry: How Cells Count and Measure Size. Annual review of biophysics vol. 45 (2016): 49-64. doi:10.1146/annurev-biophys-062215-010905
- [8] Mohapatra, Lishibanya et al. Design Principles of Length Control of Cytoskeletal Structures. Annual review of biophysics vol. 45 (2016): 85-116. doi:10.1146/annurevbiophys-070915-094206
- [9] Albus, Christin A et al. Cell length sensing for neuronal growth control. Trends in cell biology vol. 23,7 (2013): 305-10. doi:10.1016/j.tcb.2013.02.001
- [10] Folz, Frederic et al. Sound of an axon's growth. Physical review. E vol. 99,5-1 (2019): 050401. doi:10.1103/PhysRevE.99.050401
- [11] Ludington, William B et al. A systematic comparison of mathematical models for inherent measurement of ciliary length: how a cell can measure length and volume. Biophysical journal vol. 108,6 (2015): 1361-1379. doi:10.1016/j.bpj.2014.12.051
- [12] Wordeman, Linda, and Jason Stumpff. Microtubule length control, a team sport?. Developmental cell vol. 17,4 (2009): 437-8. doi:10.1016/j.devcel.2009.10.002
- [13] Melbinger, Anna et al. Microtubule length regulation by molecular motors. Physical review letters vol. 108,25 (2012): 258104. doi:10.1103/PhysRevLett.108.258104
- [14] Rank, Matthias et al. Limited Resources Induce Bistability in Microtubule Length Regulation. Physical review letters vol. 120,14 (2018): 148101. doi:10.1103/PhysRevLett.120.148101
- [15] Mohapatra, Lishibanya et al. Antenna Mechanism of Length Control of Actin Cables. PLoS computational biology vol. 11,6 e1004160. 24 Jun. 2015, doi:10.1371/journal.pcbi.1004160
- [16] Varga, Vladimir et al. Kinesin-8 motors act cooperatively to mediate length-dependent microtubule depolymerization. Cell vol. 138,6 (2009): 1174-83. doi:10.1016/j.cell.2009.07.032
- [17] Orly, Gilad et al. A Biophysical Model for the Staircase Geometry of Stereocilia. PloS one vol. 10,7 e0127926. 24 (2015), doi:10.1371/journal.pone.0127926
- [18] Patra, Swayamshree, et al. Flagellar Length Control in Biflagellate Eukaryotes: Time-of-Flight, Shared Pool, Train Traffic and Cooperative Phenomena. New Journal of Physics, vol. 22, no. 8, (2020), p. 083009., doi:10.1088/1367-2630/ab9ee4.
- [19] Prost, Jacques et al. Dynamical control of the shape and size of stereocilia and microvilli. Biophysical journal vol. 93,4 (2007): 1124-33. doi:10.1529/biophysj.106.098038
- [20] Govindan, B. S., et al. Length Control of Microtubules by Depolymerizing Motor Proteins. EPL (Europhysics Letters), vol. 83, no. 4, 2008, p. 40006., doi:10.1209/0295-5075/83/40006.
- [21] Kuan, Hui-Shun, and M D Betterton. Biophysics of filament length regulation by molecular motors. Physical biology vol. 10,3 (2013): 036004. doi:10.1088/1478-3975/10/3/036004
- [22] Reese, Louis et al. Molecular mechanisms for microtubule length regulation by kinesin-8 and XMAP215 proteins. Interface focus vol. 4,6 (2014): 20140031.

- doi:10.1098/rsfs.2014.0031
- [23] Erlenkmper, C, and K Kruse. Uncorrelated Changes of Subunit Stability Can Generate Length-Dependent Disassembly of Treadmilling Filaments. Physical Biology, vol. 6, no. 4, 2009, p. 046016., doi:10.1088/1478-3975/6/4/046016.
- [24] Fai, Thomas G et al. Length regulation of multiple flagella that self-assemble from a shared pool of components. eLife vol. 8 e42599. 9 Oct. 2019, doi:10.7554/eLife.42599
- [25] Ma, Rui et al. Speed and Diffusion of Kinesin-2 Are Competing Limiting Factors in Flagellar Length-Control Model. Biophysical journal vol. 118,11 (2020): 2790-2800. doi:10.1016/j.bpj.2020.03.034
- [26] Mogilner, A, and G Oster. Cell motility driven by actin polymerization. Biophysical journal vol. 71,6 (1996): 3030-45. doi:10.1016/S0006-3495(96)79496-1
- [27] Mogilner A, Oster G. Polymer motors: pushing out the front and pulling up the back. Curr Biol. 2003;13(18):R721-R733. doi:10.1016/j.cub.2003.08.050
- [28] McGrath, Jamis et al. Stereocilia morphogenesis and maintenance through regulation of actin stability. Seminars in cell & developmental biology vol. 65 (2017): 88-95. doi:10.1016/j.semcdb.2016.08.017
- [29] Vlez-Ortega, A Catalina, and Gregory I Frolenkov. Building and repairing the stereocilia cytoskeleton in mammalian auditory hair cells. Hearing research vol. 376 (2019): 47-57. doi:10.1016/j.heares.2018.12.012
- [30] Brown, Jeffrey W, and C James McKnight. Molecular model of the microvillar cytoskeleton and organization of the brush border. PloS one vol. 5,2 e9406. 24 Feb. 2010, doi:10.1371/journal.pone.0009406
- [31] Snell, William J et al. Cilia and flagella revealed: from flagellar assembly in Chlamydomonas to human obesity disorders. Cell vol. 117,6 (2004): 693-7. doi:10.1016/j.cell.2004.05.019
- [32] Brainina, Irina S. Applications of Random Process Excursion Analysis. Elsevier, 2017.
- [33] Kratz, Marie F. Level Crossings and Other Level Functionals of Stationary Gaussian Processes. Probability Surveys, vol. 3, 2006, pp. 230288., doi:10.1214/154957806000000087.
- [34] Rice, S. O. Mathematical Analysis of Random Noise. Bell System Technical Journal, vol. 23, no. 3, 1944, pp. 282332., doi:10.1002/j.1538-7305.1944.tb00874.x.
- [35] Rice, S. O. Mathematical Analysis of Random Noise. Bell System Technical Journal, vol. 24, no. 1, 1945, pp. 46156., doi:10.1002/j.1538-7305.1945.tb00453.x.
- [36] Milo, Ron, et al. Cell Biology by the Numbers. Garland Science, 2016.
- [37] Rafelski, Susanne M, and Wallace F Marshall. Building the cell: design principles of cellular architecture. Nature reviews. Molecular cell biology vol. 9,8 (2008): 593-602. doi:10.1038/nrm2460
- [38] Marshall, W F, and J L Rosenbaum. Intraflagellar transport balances continuous turnover of outer doublet microtubules: implications for flagellar length control. The Journal of cell biology vol. 155,3 (2001): 405-14. doi:10.1083/jcb.200106141
- [39] Chu, Fang-Yi et al. On the origin of shape fluctuations of the cell nucleus. Proceedings of the National Academy of Sciences of the United States of America vol. 114,39 (2017): 10338-10343. doi:10.1073/pnas.1702226114
- [40] Mukherji, Shankar, and Erin K O'Shea. Mechanisms of organelle biogenesis govern stochastic fluctuations in or-

- ganelle abundance. e Life vol. 3 e
02678. 10 Jun. 2014, doi:10.7554/e Life.02678
- [41] Yuan, Aidong et al. Neurofilaments and Neurofilament Proteins in Health and Disease. Cold Spring Harbor perspectives in biology vol. 9,4 a018309. 3 Apr. 2017, doi:10.1101/cshperspect.a018309
- [42] Herrmann, Harald, and Ueli Aebi. Intermediate Filaments: Structure and Assembly. Cold Spring Harbor perspectives in biology vol. 8,11 a018242. 1 Nov. 2016, doi:10.1101/cshperspect.a018242
- [43] Pollard TD, Borisy GG. Cellular motility driven by assembly and disassembly of actin filaments [published correction appears in Cell. 2003 May 16;113(4):549]. Cell. 2003;112(4):453-465. doi:10.1016/s0092-8674(03)00120-x
- [44] Borisy, Gary et al. Microtubules: 50 years on from the discovery of tubulin. Nature reviews. Molecular cell biology vol. 17,5 (2016): 322-8. doi:10.1038/nrm.2016.45
- [45] Piao, Tian et al. A microtubule depolymerizing kinesin functions during both flagellar disassembly and flagellar assembly in Chlamydomonas. PNAS vol. 106,12 (2009): 4713-8. doi:10.1073/pnas.0808671106
- [46] Masoliver, Jaume. The Level-Crossing Problem: First-Passage, Escape and Extremes. Fluctuation and Noise Letters, vol. 13, no. 04, 2014, p. 1430001., doi:10.1142/
- [47] Ghusinga, Khem Raj et al. First-passage time approach to controlling noise in the timing of intracellular events. Proceedings of the National Academy of Sciences of the United States of America vol. 114,4 (2017): 693-698. doi:10.1073/pnas.1609012114
- [48] Thorneywork, Alice L., et al. Direct Detection of Molecular Intermediates from First-Passage Times. 2019, doi:10.1101/772830.
- [49] Dhar, Abhishek, et al. Run-and-Tumble Particle in One-Dimensional Confining Potentials: Steady-State, Relaxation, and First-Passage Properties. Physical Review E, vol. 99, no. 3, 2019, doi:10.1103/physreve.99.032132.
- [50] Besga, Benjamin, et al. Optimal Mean First-Passage Time for a Brownian Searcher Subjected to Resetting: Experimental and Theoretical Results. Physical Review Research, vol. 2, no. 3, 2020, doi:10.1103/physrevresearch.2.032029.
- [51] Ghosh, Soumendu, et al. First-Passage Processes on a Filamentous Track in a Dense Traffic: Optimizing Diffusive Search for a Target in Crowding Conditions. Journal of Statistical Mechanics: Theory and Experiment, vol. 2018, no. 12, 2018, p. 123209., doi:10.1088/1742-5468/aaf31d.
- [52] Bel, G., Zilman, A. & Kolomeisky, A.B. Different time scales in dynamic systems with multiple exits. (2020) arXiv:2006.10613
- [53] Evans, Martin R, and Satya N Majumdar. Diffusion with Resetting in Arbitrary Spatial Dimension. Journal of Physics A: Mathematical and Theoretical, vol. 47, no. 28, 2014, p. 285001., doi:10.1088/1751-8113/47/28/285001.
- [54] Zhang, Yaojun, and Olga K Dudko. First-Passage Processes in the Genome. Annual review of biophysics vol. 45 (2016): 117-34. doi:10.1146/annurev-biophys-062215-010925
- [55] Polizzi, Nicholas F et al. Mean First-Passage Times in Biology. Israel journal of chemistry vol. 56,9-10 (2016): 816-824. doi:10.1002/ijch.201600040
- [56] Metzler, R., Oshanin, G., &; Redner, S. (2014). First-passage phenomena and their applications. New Jersey: World Scientific.

- [57] IyerBiswas, S. and Zilman, A. (2016). FirstPassage Processes in Cellular Biology. In Advances in Chemical Physics (eds S.A. Rice and A.R. Dinner). doi:10.1002/9781119165156.ch5
- [58] Guillet, A., Roldan, E., Julicher , F., Extreme-Value Statistics of Molecular Motors arXiv preprint arXiv:1908.03499 (2019)
- [59] Greulich, P., &; Simons, B. D. (2018). Extreme value statistics of mutation accumulation in renewing cell populations. Physical Review E, 98(5). doi:10.1103/physreve.98.050401
- [60] Syski, Ryszard. Passage Times for Markov Chains. IOS Press, 1992.
- [61] Stratonovic R. L. Topics in the Theory of Random Noise. Gordon and Breach, 1981.
- [62] Malakar, Kanaya, et al. Steady State, Relaxation and First-Passage Properties of a Run-and-Tumble Particle in One-Dimension. Journal of Statistical Mechanics: Theory and Experiment, vol. 2018, no. 4, 2018, p. 043215., doi:10.1088/1742-5468/aab84f.
- [63] Zacks, Shelemyahu. Sample Path Analysis and Distributions of Boundary Crossing Times. Springer International Publishing, 2017.
- [64] Bressloff, Paul C. Stochastic Processes in Cell Biology. Springer International Publishing, 2014.
- [65] Kampen, N. G. van. Stochastic Processes in Physics and Chemistry. World Publishing Corporation, 2010.
- [66] Gardiner, Crispin W. Stochastic Methods: a Handbook for the Natural and Social Sciences. Springer, 2009.
- [67] Weisstein, Eric W. "Erfi." From Math-World - A Wolfram Web Resource. https://mathworld.wolfram.com/Erfi.html
- [68] Banerjee, Deb Sankar, and Shiladitya Banerjee. Size Regulation of Multiple Organelles Competing for a Shared Subunit Pool. 2020, doi:10.1101/2020.01.11.902783.
- [69] Gillespie, Daniel T., and Effrosyni Seitaridou. Simple Brownian Diffusion: an Introduction to the Standard Theoretical Models. Oxford University Press, 2013.
- [70] Abramowitz, Milton, and Irene A. Stegun. Handbook of Mathematical Functions with Formulas, Graphs, and Mathematical Tables. U.S. Dept. of Commerce, National Bureau of Standards, 1972.
- [71] Hartich, David, and Alja Godec. Extreme Value Statistics of Ergodic Markov Processes from First Passage Times in the Large Deviation Limit. Journal of Physics A: Mathematical and Theoretical, vol. 52, no. 24, 2019, p. 244001., doi:10.1088/1751-8121/ab1eca.
- [72] K.F. Lechtrack, J.C. Van De Weghe, J.A. Harris and P. Liu, Protein transport in growing and steady-state cilia, Traffic 18, 277-286 (2017).
- [73] B.D. Engel, W.B. Ludington and W.F. Marshall, Intraflagellar transport particle size scales inversely with flagellar length: revisiting the balance-point length control model, J. Cell Biol. 187, 81-89 (2009).
- [74] K.G. Kozminski, K.A. Johnson, P. Forscher and J.L. Rosenbaum, A motility in the eukaryotic flagellum unrelated to flagellar beating, PNAS 90, 5519-5523 (1993).
- [75] K.G. Kozminski, Intraflagellar transport- the "new motility" 20 years later, Mol. Biol. Cell 23, 751-753 (2012).
- [76] J.L. Rosenbaum and G.B. Witman, *Intraflagellar transport*, Nat. Rev. Mol. Cell Biol. **3**, 813 (2002).
- [77] L. Stepanek and G. Pigino, Microtubule doublets are double-track railways for Intraflagellar transport trains, Science. 352, 721-4 (2016).

[78] H. Ishikawa and W.F. Marshall, Testing the time-of-flight model for flagellar length sensing, Mol. Biol. Cell 28,

3447-3456 (2017).